UNIVERSITÉ DE GENÈVE

Archive ouverte UNIGE
https://archive-ouverte.unige.ch

Article scientifique | Article | 2018

Accepted version | Open Access

This is an author manuscript post-peer-reviewing (accepted version) of the original publication. The layout of the published version may differ .

Deciphering the Influence of Meridional versus Facial Isomers in Spin Crossover Complexes

Lathion, Timothee; Guenee, Laure; Besnard, Céline; Bousseksou, Azzedine; Piguet, Claude

How to cite

LATHION, Timothee et al. Deciphering the Influence of Meridional versus Facial Isomers in Spin Crossover Complexes. In: Chemistry - A European Journal, 2018, vol. 24, n° 63, p. 16873–16888. doi: 10.1002/chem.201804161

This publication URL: https://archive-ouverte.unige.ch/unige:111518

Publication DOI: 10.1002/chem.201804161

© This document is protected by copyright. Please refer to copyright holder(s) for terms of use.

Publication: Chem. Eur. J. 2918, 24, 16873-16888

CHEMISTRY
A European Journal

A Journal of
ChemPubSoc Europe

Accepted Article

Title: Deciphering the Influence of Meridional vs Facial Isomers in Spin Crossover Complexes

Authors: Claude Piguet, Timothée Lathion, Laure Guénée, Céline Besnard, and Azzedine Bousseksou

This manuscript has been accepted after peer review and appears as an Accepted Article online prior to editing, proofing, and formal publication of the final Version of Record (VoR). This work is currently citable by using the Digital Object Identifier (DOI) given below. The VoR will be published online in Early View as soon as possible and may be different to this Accepted Article as a result of editing. Readers should obtain the VoR from the journal website shown below when it is published to ensure accuracy of information. The authors are responsible for the content of this Accepted Article.

To be cited as: *Chem. Eur. J.* 10.1002/chem.201804161

Link to VoR: http://dx.doi.org/10.1002/chem.201804161

Supported by
ACES

WILEY-VCH

Deciphering the Influence of Meridional *vs* Facial Isomers in Spin Crossover Complexes.

Timothée Lathion,[a] Laure Guénée,[b] Céline Besnard,[b] Azzedine Bousseksou[c] and Claude Piguet*[a]

---

[a] *Dr T. Lathion, Prof. Dr C. Piguet. Department of Inorganic and Analytical Chemistry, University of Geneva, 30 quai E. Ansermet, CH-1211 Geneva 4 (Switzerland). E-mail: Claude.Piguet@unige.ch*

[b] *Dr L. Guénée, Dr C. Besnard. Laboratory of Crystallography, University of Geneva, 24 quai E. Ansermet, CH-1211 Geneva 4 (Switzerland)*

[c] *Dr A. Bousseksou. Laboratory of Coordination Chemistry (LCC), CNRS & Université de Toulouse (UPS, INP), 205 route de Narbonne, Toulouse 31077 Cedex 4 (France).*

Supporting information and the ORCID identification number(s) for the author(s) of this article can be found under https://doi.org/10.1002/chemxxxxx

Accepted Manuscript

This article is protected by copyright. All rights reserved.

Abstract

Chelate coordination of non-symmetrical didentate pyrazine-benzimidazole (**L1**) or pyridine-benzimidazole (**L2**) *N*-donor ligands around divalent iron in acetonitrile produces stable homoleptic triple-helical spin crossover $[Fe(\mathbf{L}\boldsymbol{k})_3]^{2+}$ complexes existing as mixtures of meridional (C_1-symmetry) and facial (C_3-symmetry) isomers in slow exchange on the NMR time scale. The speciation deviates from the expected statistical ratio *mer*/*fac* = 3:1, a trend assigned to the thermodynamic *trans*-influence combined with solvation effects. Consequently, the observed spin state $Fe^{II}_{low\text{-}spin} \leftrightarrow Fe^{II}_{high\text{-}spin}$ equilibria occurring in $[Fe(\mathbf{L}\boldsymbol{k})_3]^{2+}$ refer to mixtures of complexes in solution, an issue usually not considered in this field, but which limits rational structure-properties correlations. Taking advantage of the selective and quantitative formation of isostructural facial isomers in non-constrained related spin crossover d-f helicates (HHH)-$[LnFe(\mathbf{L}\boldsymbol{k})_3]^{5+}$ (Ln is a trivalent lanthanide, **L*k*** = **L5**, **L6**), we propose a novel strategy for assigning pertinent thermodynamic driving forces to each spin crossover triple-helical isomer. The different enthalpic contributions to the spin state equilibrum found in *mer*-$[Fe(\mathbf{L}\boldsymbol{k})_3]^{2+}$ and *fac*-$[Fe(\mathbf{L}\boldsymbol{k})_3]^{2+}$ reflect the Fe-N bond strengths dictated by the *trans*-influence, while a concomitant solvent-based entropic contribution reinforces the latter effect and results in systematic shifts of the spin crossover transitions toward higher temperature in the facial isomers.

Introduction

Almost nine decades after the discovery of the spin state equilibrium phenomenon,[1] a plethora of d^4-d^7 complexes has been identified for their spin crossover properties, which can be induced by thermal, pressure, optical or pH stimuli.[2] Among them, the d^6 pseudo-octahedral six-coordinate $[Fe^{II}N_6]$ chromophore[3] found in $[Fe\mathbf{L}_3]$ (**L** is a didentate *N*-donor ligand) and in $[Fe(\mathbf{L'})_2]$ (**L'** is a tridentate *N*-donor ligand) plays a central role.[4] Taking pure octahedral symmetry (O_h) as a guide for $[FeN_6]$ entities, the electronic ground state of the Fe^{II} center 'hesitates' between low-spin (ls) and high-spin (hs) configurations depending on the balance between the magnitude of the ligand-field strength Δ_{oct} and that of the electron spin pairing energy *P* (Scheme 1).

Accepted Manuscript

This article is protected by copyright. All rights reserved.

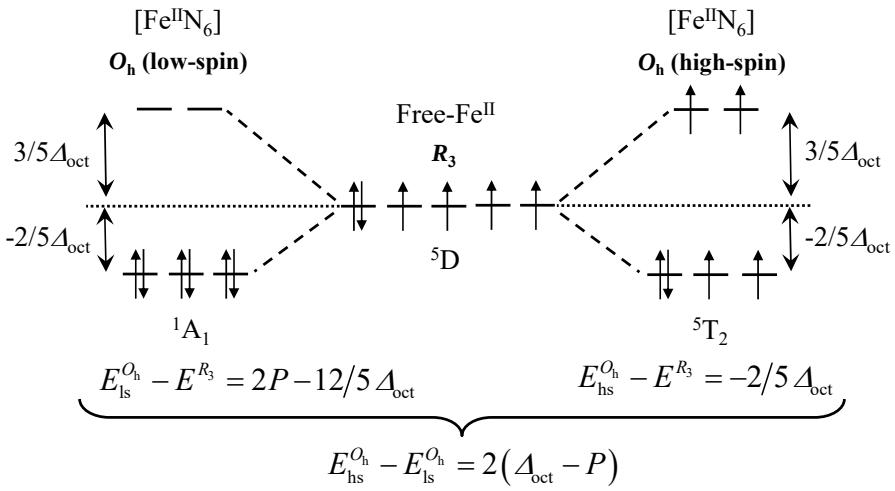

Scheme 1. The thermodynamic origin of Fe^{II} spin state equilibria in octahedral symmetry (*P* is the electron spin pairing energy).

Since both the spectrophotometric series (which controls Δ_{oct})[5] and the nephelauxetic series (which controls *P* via the Racah parameters *B* and *C*)[6] depend on the strength and on the nature of the metal-ligand interactions, it is not so surprising that, for $[FeN_6]$ units, the coordination sphere of which is systematically made up of six heterocyclic nitrogen donor, some simple metric parameters were found to be valuable reporters for predicting the emergence of either pure low-spin state ($\left(E_{hs}^{O_h} - E_{ls}^{O_h}\right) >> RT$), pure high-spin state ($\left(E_{ls}^{O_h} - E_{hs}^{O_h}\right) >> RT$) or spin state equilibria ($\left|E_{hs}^{O_h} - E_{ls}^{O_h}\right| \approx RT$, Eq. (1)).[7]

$$Fe^{II}_{low\text{-}spin} \rightleftharpoons Fe^{II}_{high\text{-}spin} \qquad K_{SCO} = x_{hs}/x_{ls} = e^{-(\Delta G_{SCO}/RT)} = e^{(\Delta S_{SCO}/R - \Delta H_{SCO}/RT)} \qquad (1)$$

In the famous family of homoleptic tris-diimine complexes $[Fe\mathbf{L}_3]^{2+}$, the interatomic distance *d*(N···N) between the two *N*-donor atoms in the non-coordinated didentate diimine ligands proved to be the searched indicator for predicting spin crossover (SCO) behaviors.[7] Values of *d*(N···N) larger than 2.91 Å, as found in non-constrained didentate ligands made up of connected five-membered ring/five-membered ring (for instance 2,2'-biimidazole), produce loose Fe-N bonding and high-spin ground states. On the contrary, *d*(N···N) distances smaller than 2.75 Å as found in 2,2'-bipyridine, the archetype of two connected six-membered ring/six-membered ring, strongly stabilize low-spin configurations. Spin crossover behaviors match the intermediate regime ($2.75 \leq d(N\cdots N) \leq 2.91$ Å)

Accepted Manuscript

This article is protected by copyright. All rights reserved.

provided by non-symmetrical didentate ligands made up of connected five-membered ring/six-membered ring as found in 2,2'-pyridine-imidazole or derivatives of it.[7] Taking now for granted that favorable metric parameters are in hand, some further tuning of the thermodynamic SCO parameters (Eq. (1)) results from the modulation of specific σ-donating (mainly affecting Δ_{oct}) and/or π-accepting characteristics (mainly affecting the spin pairing energy P via the Racah parameter B) encoded in the bound heterocyclic rings. Reminiscent of *Tanabe-Sugano* diagrams,[8] the trivial thermodynamic analysis summarized in Scheme 1 implies that the spin crossover properties in Fe^{II} complexes depend on the Δ_{oct}/B ratio where (i) large values favor low-spin configurations, (ii) small values stabilize high-spin states and (iii) intermediate values induce SCO behaviors. A precise and rational correlation between molecular ligand structures and thermodynamic ΔH_{SCO}, ΔS_{SCO} parameters (especially the equilibrium temperature $T_{1/2} = \Delta H_{SCO}/\Delta S_{SCO}$) thus goes through the Δ_{oct}/B ratio, a crucial strategy for the rational programming of accessible spin state transitions, which can be implemented in magnetic[9] and/or optical[10] (nano)molecular switches for practical applications. With this goal in mind, major efforts were focused on the systematic synthesis of large collections of didentate and tridentate polyimine binding units with variable coordinating properties for tuning the SCO transition temperatures and thermodynamic cooperativities in $[Fe\mathbf{L}_3]^{2+}$ and $[Fe(\mathbf{L'})_2]^{2+}$ complexes.[2]-[4],[9],[10] Although unsymmetrical didentate ligands have been often reacted with Fe^{II} to give triple-helical homoleptic $[Fe\mathbf{L}_3]^{2+}$ complexes, the influence of standard meridional and facial isomerization on the spin state equilibrium mainly escaped attention and interest (Figure 1). Only a few salts containing a single isomer could be isolated in the solid state (meridional or facial as certified by their X-ray crystal structures),[11] but the associated SCO parameters did not give any clear evidences or trends, probably because intermolecular packing interactions responsible for the stabilization of the crystal structures largely dominate minor molecular effects. To the best of our knowledge, no attempt was made to address the meridional/facial challenge in solution where the limited solvation effects offer the opportunity to establish direct links between molecular geometries and SCO properties.

Accepted Manuscript

This article is protected by copyright. All rights reserved.

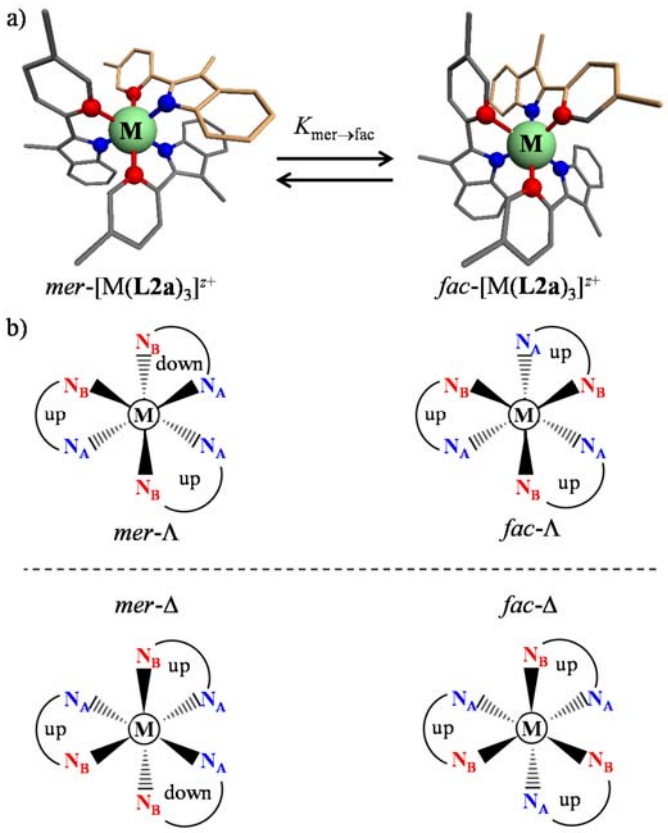

Figure 1. a) Perspective view along the helical axis for the meridional→facial isomerization processes (flip of the yellow ligand) operating in homoleptic [M(**L2a**)$_3$]$^{z+}$ complex where **L2a** is the archetype of a non-symmetrical didentate ligand (see Scheme 2) and M is a pseudo-octahedral six-coordinate metal center. b) Schematic views of the two enantiomeric pairs of *mer*/*fac* geometrical isomers.

Pioneer attempts to address this challenge aim at connecting three unsymmetrical didentate units to a short hydrocarbon-containing tripod, thus producing sexidentate ligands **L"**, which force the formation of the facial isomer *fac*-[Fe**L"**]$^{2+}$ as the unique complex in solution.[4d],[7],[12] However, this strategy induces drastic intramolecular thermodynamic constraints during the formation of the [FeN$_6$] chromophore, an effect which can be quantified with the help of the concept of effective molarity.[13] Applied to related podands bound to more flexible trivalent lanthanides, free-energy penalties as large as 70-80 kJ/mol are common for the preorganization of three unsymmetrical binding units by short to medium-size tripods. Compared with a total binding energy of 110-120 kJ/mol accounting for pure intermolecular processes, this facial organization in a single tripodal ligand corresponds to *c.a.* 60% reduction of the affinity for the entering metal.[14] One therefore understands why such constrained

Accepted Manuscript

This article is protected by copyright. All rights reserved.

tripodal complexes were not further considered as fair models for extracting the SCO properties of analogous, but unconstrained *fac*-$[Fe\mathbf{L}_3]^{2+}$ isomers. However, some recent progresses made in the understanding of the thermodynamic *trans*-influence occuring in simple mononuclear *mer*/*fac*-$[Zn(\mathbf{L}\boldsymbol{k})_3]^{2+}$ isomers (**L*k*= L1**, **L2**; Scheme 2 top)[15] combined with the design of flexible non-covalent tripods displaying minor intramolecular cost (≤ 20 kJ/mol) in *HHH*-$[ZnLn(\mathbf{L}\boldsymbol{k})_3]^{5+}$ helicates (**L*k*= L5**, **L6**; Scheme 2 bottom),[16] reactivate the search for a rational treatment of the influence of molecular *mer*-$[Fe\mathbf{L}_3]^{2+}$ ↔ *fac*-$[Fe\mathbf{L}_3]^{2+}$ isomerization on the SCO properties of these complexes in solution. We report here on the discovery that the meridional and facial isomers, due to their structural differences indeed display synergestic enthalpic and entropic contributions, which may shift the spin crossover transition temperature $T_{1/2}$ by up to 60 degrees. A thermodynamic analysis assigns this effect to *trans*-influence and to changes in (dipole-based) solvation energies accompanying the change in volume produced by the SCO reaction.

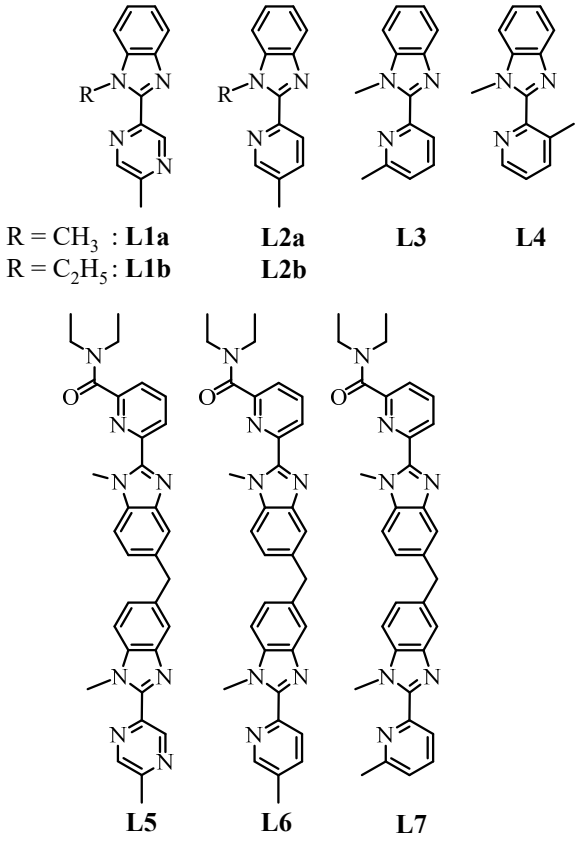

Scheme 2. Chemical structures of ligands **L1-L7** considered in this work.

Accepted Manuscript

This article is protected by copyright. All rights reserved.

Experimental section

Chemicals were purchased from Sigma-Aldrich and Acros and used without further purification unless otherwise stated. The didentate ligands **L1**,[15] **L2**,[15] **L3**,[17] and segmental ligands **L5**,[15] **L6** [18] and **L7** [19] were prepared according to literature procedures. Dichloromethane, diethyl ether and *N,N*-dimethylformamide were dried through an alumina cartridge. Silica-gel plates (Merck, 60 F_{254}) were used for thin-layer chromatography, SiliaFlash® silica gel P60 (0.04-0.063 mm,) and Acros silica gel 60 (0.035-0.07 mm) were used for preparative column chromatography.

Preparation of *N*-methyl-2-nitroaniline (1). 1-chloro-2-nitrobenzene (31.75 g, 201.5 mmol, 1.0 eq) and methylamine (198 mL, 40% wt in H_2O, 2295.6 mmol, 11.4 eq) were introduced into a Carius tube equipped with a magnetic stirrer, and heated at 120 °C for 48 h. Excess of methylamine was rotatory evaporated and the residual brown oil was partitioned between CH_2Cl_2 (300 mL) and half sat. aq. NH_4Cl (300 mL). The organic layer was separated and the aq. phase was further extracted with CH_2Cl_2 (3 x 150 mL). The combined organic extracts were dried over anhydrous Na_2SO_4, filtered and the solvent evaporated to dryness. The resulting red oil was purified by column chromatography (silica, CH_2Cl_2) to give 28.99 g of *N*-methyl-2-nitroaniline (**1**, 190.5 mmol, yield 94.5 %) as a deep red orange oil, which slowly crystallized within hours. ^{1}H NMR ($CDCl_3$, 400 MHz, 298 K) δ ppm : 8.13 (1H, dd, ^3J = 8.8 Hz, ^4J = 1.6 Hz), 8.00 (1H, bs), 7.43 (1H, ddd, ^3J = 8.8 Hz, ^3J = 7.2 Hz, ^4J = 1.6 Hz), 6.81 (1H, dd, ^3J = 8.6 Hz, ^4J = 1.0 Hz), 6.62 (1H, ddd, ^3J = 8.4 Hz, ^3J = 7.2 Hz, ^4J = 1.2 Hz), 2.99 (3H, s).

Preparation of 3-methyl-picolinic acid (2). 3-methyl-picolinonitrile (1.53 g, 13.0 mmol, 1.0 eq) in aq. 5M NaOH (5 mL) were refluxed for 4 h. After cooling, the mixture was neutralized (pH = 2.0) with concentrated hydrochloric acid (12 M) and evaporated to dryness. The residual solid was suspended in ethyl acetate (250 mL), refluxed for 3 h and filtered when hot through a Büchner funnel. The filtrate was evaporated to dryness to give 1.61 g of 3-methyl-picolinic acid (**2**, 11.7 mmol, yield 91 %) as a white powder. ^{1}H NMR ($CDCl_3$, 400 MHz, 298 K) δ ppm: 9.97 (1H, bs), 8.46 (1H, dd, ^3J = 4.8 Hz, ^4J = 0.8 Hz), 7.72 (1H, dd, ^3J = 7.8 Hz, ^4J = 0.6 Hz), 7.48 (1H, dd, ^3J = 7.8 Hz, ^3J = 4.6 Hz), 2.78 (3H, s). RMN ^{1}H ($(CD_3)_2SO$, 400 MHz, 298 K) δ ppm: 13.07 (1H, s), 8.46 (1H, dd, ^3J =

Accepted Manuscript

This article is protected by copyright. All rights reserved.

4.6 Hz, ^4J = 1.0 Hz), 7.77 (1H, d, ^3J = 8.0 Hz), 7.47 (1H, dd, ^3J = 7.8 Hz, ^3J = 4.6 Hz), 2.46 (3H, s). ^{13}C NMR ($CDCl_3$, 100 MHz, 298 K) δ ppm: 164.40 (C_q), 145.32 (CH), 143.39 (C_q), 141.80 (CH), 137.67 (C_q), 129.79 (CH), 20.30 (CH_3).

Preparation of *N*,3-dimethyl-*N*-(2-nitrophenyl)picolinamide (3). Thionyl chloride (4.8 mL, 66.1 mmol, 6.0 eq) were dropwise added to a mixture of 3-methyl-picolinic acid (**2**, 1.51 g, 11.0 mmol, 1.0 eq) and *N*,*N*-dimethylformamide (200 µl) in dry 1,2-dichloroethane (10 mL). The solution was refluxed for 4 h under an inert atmosphere, then cooled and evaporated to dryness. The residue was dissolved in dry CH_2Cl_2 (15 mL) and a solution of *N*-methyl-2-nitroaniline (**1**, 4.41 g, 27.2 mmol, 2.5 eq) in dry CH_2Cl_2 (10 mL) was added dropwise. The final mixture was refluxed for 14 h during which two portions of (iPr)$_2$NEt (3 mL, 17.2 mmol, 1.6 eq) were added after 20 min and 12 h, respectively. Evaporation to dryness provided a solid, which was partitioned between CH_2Cl_2 (200 mL) and half sat. aq. NH_4Cl (200 mL). The organic layer was separated and the aq. phase was further extracted with CH_2Cl_2 (3 x 120 mL). The combined organic extracts were dried over anhydrous Na_2SO_4, filtered and the solvent evaporated to dryness to give 2.38 g of *N*,3-dimethyl-*N*-(2-nitrophenyl)picolinamide (**3**, 8.8 mmol, yield 80 %) as a brownish solid. ^{1}H NMR ($CDCl_3$, 400 MHz, 298 K) δ ppm: mixture of rotamers A (2/3) et B (1/3): 8.50-7.50 (4H, m), 7.48-6.95 (3H, m), 3.56 (3H, s, A), 3.28 (3H, s, B), 2.44 (3H, s, B), 2.38 (3H, s, A). ESI-MS (soft positive mode, *m*/*z*): [**3**+H]$^+$: 272.1 (exp.), 272.3 (calc.); [(**3**)$_2$+H]$^+$: 543.8 (exp.), 543.6 (calc.).

Preparation of ligand L4. *N*,3-dimethyl-*N*-(2-nitrophenyl)picolinamide (**3**, 2.38 g, 8.8 mmol, 1.0 eq) and activated powdered iron (9.77 g, 174.9 mmol, 19.9 eq) were refluxed for 24 h in a mixture of ethanol (400 mL), water (115 mL) and concentrated hydrochloric acid (37 % in H_2O, 25 mL, 294.3 mmol, 33.5 eq). Excess iron was removed with a magnet and ethanol was evaporated. Water (50 mL) and EDTA disodium dihydrate (65.3 g, 175.4 mmol, 20.0 eq) in water (250 mL) were successively added to the solution and its pH was adjusted to 9.5 with concentrated aq. ammonia. CH_2Cl_2 (300 mL) was finally added together with concentrated hydrogen peroxide (30 % in H_2O, 5 mL, 44.1 mmol, 5.0 eq) in small portions under vigorous stirring. The organic layer was separated and the aq.

Accepted Manuscript

This article is protected by copyright. All rights reserved.

phase was further extracted with CH_2Cl_2 (3 x 300 mL). The combined organic extracts were dried over anhydrous Na_2SO_4, filtered and the solvent evaporated to dryness. The solid residue was purified by column chromatography (silica, CH_2Cl_2/MeOH 98:2) to give 1.45 g of **L4** (6.5 mmol, yield 74 %) as a cream powder. ^{1}H NMR ($CDCl_3$, 400 MHz, 298 K) δ ppm: 8.58 (1H, dd, ^3J = 4.6 Hz, ^4J = 0.6 Hz), 7.85-7.83 (1H, m), 7.70 (1H, d, ^3J = 7.6 Hz), 7.45-7.43 (1H, m), 7.38-7.29 (3H, m), 3.88 (3H, s), 2.56 (3H, s). ^{13}C NMR ($CDCl_3$, 100 MHz, 298 K) δ ppm: 150.94 (C_q), 148.69 (C_q), 146.52 (CH), 142.62 (C_q), 139.02 (CH), 135.83 (C_q), 135.04 (C_q), 123.79 (CH), 123.03 (CH), 122.24 (CH), 120.11 (CH), 109.69 (CH), 31.39 (CH_3), 19.58 (CH_3). ESI-MS (soft positive mode, m/z) : [**L4**+H]$^+$: 224.4 (exp.), 224.3 (calc.). Elemental analysis: calcd: %C 75.31, %H 5.87, %N 18.82 ; found: %C 75.16, %H 5.83, %N 19.02.

Preparation of mononuclear Fe^{II} complexes with L1-L4. In a typical synthesis, 1.47 mmol of ligand **L*k*** (3.0 eq) in CH_2Cl_2 (8 mL) were added to 0.49 mmol (1.0 eq) of $Fe(CF_3SO_3)_2$ or $Fe(BF_4)_2{\cdot}6H_2O$ in acetonitrile (48 mL). The resulting mixture was stirred for 12 h under argon, then evaporated to dryness. The solid residue was dissolved in acetonitrile (4 mL) and diethylether was slowly diffused until the formation of microcrystalline powders or monocrystals suitable for X-ray diffraction studies. Filtration followed by washing with diethyl ether gave 62-85 % of [Fe(**L*k***)$_3$]$(CF_3SO_3)_2{\cdot}x$Solvent or [Fe(**L*k***)$_3$]$(BF_4)_2{\cdot}x$Solvent. For the hexafluorofluorophosphate salt, the same procedure was repeated in presence of (^{n}Bu)$_4$NPF$_6$ (25 eq) to yield 59-82% of [Fe(**L*k***)$_3$]$(PF_6)_2{\cdot}x$Solvent. All complexes were characterized by elemental analyses (Table S1 Supporting Information) and X-ray crystal structures could be solved for [Fe(**L2a**)$_3$]$(PF_6)_2$ (**4**) and [Fe(**L4**)$_3$]$(ClO_4)_2{\cdot}CH_3CN$ (**5**). The latter complex was crystallized in presence of a large excess of (^{n}Bu)$_4$NClO$_4$.

Caution! *Dry perchlorates may explode and should be handled in small quantities and with the necessary precautions.*[20]

Preparation of dinuclear Ln^{III}Fe^{II} and Ln^{III}Zn^{II} complexes with L5-L7. In a typical synthesis, 27.6 μmol of $Ln(CF_3SO_3)_3$ (1.0 eq; Ln = La or Eu) and 27.6 μmol of $M(CF_3SO_3)_2$ (1.0 eq; M = Fe or Zn)

Accepted Manuscript

This article is protected by copyright. All rights reserved.

in acetonitrile/water (99:1, 1.38 mL) were added to 82.8 μmol of ligand **L*k*** (3 eq) in dichloromethane (700 μl) and the resulting clear solution was stirred for 4 h under an inert atmosphere. The solvent were removed and the solid residue was dissolved in acetonitrile (2 mL). Diethylether was slowly diffused until the formation of microcrystalline powders or monocrystals suitable for X-ray diffraction studies. Filtration followed by washing with diethyl ether gave 68-93 % of $[LnFe(\mathbf{L}\boldsymbol{k})_3](CF_3SO_3)_5{\cdot}x$Solvent or $[LnZn(\mathbf{L}\boldsymbol{k})_3](CF_3SO_3)_5{\cdot}x$Solvent. For the hexafluorofluorophosphate, the same procedure was repeated in presence of $(^n Bu)_4NPF_6$ (25 eq) to yield 69-87% of $[LnFe(\mathbf{L}\boldsymbol{k})_3](PF_6)_5{\cdot}x$Solvent. All complexes were characterized by elemental analyses (Table S2 Supporting Information). Single crystal X-ray crystal structures could be solved for $[LaFe(\mathbf{L5})_3](ClO_4)_5{\cdot}5CH_3CN$ (**6**), $[EuFe(\mathbf{L5})_3](ClO_4)_5{\cdot}6CH_3CN$ (**7**), $[EuFe(\mathbf{L6})_3](CF_3SO_3)_5{\cdot}2.5CH_3CN{\cdot}(CH_3)_3C(OCH_3)$ (**8**), $\{[LaFe(\mathbf{L7})_3](ClO_4)_5\}_2{\cdot}6CH_3CN{\cdot}1.5H_2O$ (**9**), $\{[EuFe(\mathbf{L7})_3](CF_3SO_3)_5\}_2{\cdot}4CH_3CN{\cdot}3(CH_3)_3C(OCH_3)$ (**10**) and $[LuFe(\mathbf{L7})_3](CF_3SO_3)_5{\cdot}2CH_3CN$ (**11**). The perchlorate complexes were crystallized in presence of a large excess of $(^n Bu)_4NClO_4$.

Spectroscopic and analytical measurements

^1H and ^{13}C NMR spectra were recorded at 293 K on a Bruker Avance 400 MHz spectrometer. Chemical shifts are given in ppm with respect to TMS. Spectrophotometric titrations were performed with a J&M diode array spectrometer (Tidas series) connected to an external computer. In a typical experiment, 25 cm^3 of ligand in acetonitrile ($2{\cdot}10^{-4}$ M) were titrated at 298 K with a solution of $Fe(CF_3SO_3)_2$ ($2{\cdot}10^{-3}$ M) in acetonitrile under an inert atmosphere. After each addition of 75 μL, the absorbance was recorded using Hellma optrodes (optical path length 0.1 cm) immersed in the thermostated titration vessel and connected to the spectrometer. Mathematical treatment of the spectrophotometric titrations was performed with factor analysis[21] and with ReactLab™ Equilibria (previously Specfit/32).[22] Pneumatically-assisted electrospray (ESI-MS) mass spectra were recorded from 10^{-4} M (ligands) and 10^{-3} M (complexes) solutions on an Applied Biosystems API 150EX LC/MS System equipped with a Turbo Ionspray source. Elemental analyses were performed by K. L. Buchwalder from the Microchemical Laboratory of the University of Geneva. Electronic spectra in

Accepted Manuscript

This article is protected by copyright. All rights reserved.

the UV-Vis region were recorded at 293 K from solutions in CH_3CN with a Perkin-Elmer Lambda 1050 using quartz cells of 0.1 or 1.0 mm path length. Solid-state magnetic data were recorded on a MPMS 3 or MPMS 5 QUANTUM DESIGN magnetometers using magnetic fields of 1000-5000 Oe and at 2 K/min rates within the 2-400 K range. The magnetic susceptibilities were corrected for the magnetic response of the sample holder and for the diamagnetism of the compounds.[23] Magnetic data for samples in acetonitrile were obtained by the Evans method[24] using methanol for temperature calibration.[25] The method was modified for application with a superconducting magnet.[26] Specific problems associated with the 'solvent correction term'[27] were overcome by determining the diamagnetic contribution under the same experimental conditions.[28] Measurements were carried out on degassed CD_3CN solutions containing 1% (v/v) and using tert-butanol as an internal reference. All the data were corrected for changes in solvent density with temperature.[29]

X-ray crystallography

Single crystals. Summary of crystal data, intensity measurements and structure refinements for compounds (**4**) to (**11**) were collected in Tables S3-S10. The crystals were mounted on MiTeGen kapton cryoloops with protection oil. X-ray data collections were performed with an Agilent SuperNova Dual diffractometer equipped with a CCD Atlas detector (Cu[Kα] radiation). The structures were solved by using direct methods.[30] Full-matrix least-square refinements on F^2 were performed with SHELX2014.[31] CCDC 1862027-1862034 contain the supplementary crystallographic data. These data can be obtained free of charge from the Cambridge Crystallographic Data Centre via www.ccdc.cam.ac.uk/.

Powder crystals. Variable temperature X-ray powder diffraction experiments were performed on an Empyrean (PANalytical) diffractometer in capillary mode, with a focusing X-ray mirror for $Cu_{K\alpha}$ radiation and a PIXcel3D area detector. Variable temperatures were achieved with a nitrogen cryostreamer (Oxford cryosystem). Temperature cooling ramps from 340 K to 140 K were performed at 3 $K \cdot min^{-1}$ and data collections were performed at fixed temperature plateau (2theta range from 7 to 30° with continuous scan total time 26 min/diagram)

Accepted Manuscript

This article is protected by copyright. All rights reserved.

Results and Discussions

Solid-state SCO Fe(II) complexes with ligands L1-L7: an empirical approach.

The didentate ligands **L1**-**L2**[15] and **L3**[17] were previously obtained according to standard *Phillips*-modified strategies similar to that used for the novel ligand **L4** (Scheme 3). 3-methyl-picolinic acid (**2**) was in situ activated as its acid chloride, which was further reacted with *N*-methyl-2-nitroaniline (**1**) to give the ortho-nitroamide (**3**) in good yield. Final reductive cyclization provided the target constrained ligand **L4**.

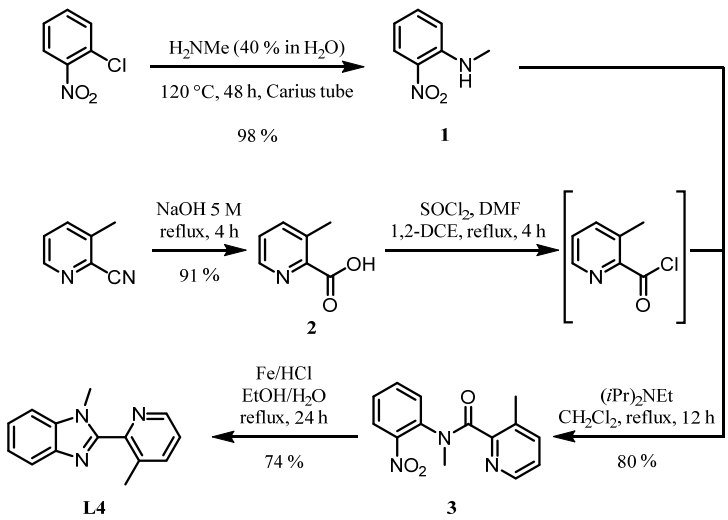

Scheme 3. Multistep synthesis of ligand **L4**.

Stoichiometric reactions of **L1**-**L4** (3.0 eq) with $Fe(CF_3SO_3)_2$ or $Fe(BF_4)_2$ (1.0 eq) in dichloromethane/acetonitrile mixtures followed by slow diffusion of volatile ether provided fair yields (62-85%) of microcrystalline $[Fe(\mathbf{L}\boldsymbol{k})_3](CF_3SO_3)_2$ and $[Fe(\mathbf{L4})_3](BF_4)_2$ complexes with various amounts of co-crystallized solvent molecules (Table S1 in the Supporting Information). Subsequent metathesis of the triflate anions with the help of $(^n Bu)_4NPF_6$ in acetonitrile/ether mixtures additionally yielded $[Fe(\mathbf{L}\boldsymbol{k})_3](PF_6)_2$ (**L*k*** = **L1a**, **L2a**, **L4**, Table S1). Intense efforts for producing mono-crystals of sufficient quality for X-ray diffraction studies were only successful for $[Fe(\mathbf{L2a})_3](PF_6)_2$ (**4**) and $[Fe(\mathbf{L4})_3](ClO_4)_2{\cdot}CH_3CN$ (**5**, after methathesis with $(^n Bu)_4NClO_4$, Figure 2 top, Tables S3-S4 and Figures S1-S2 in the Supporting Information). The six-coordinate homoleptic tris-diimine $[Fe(\mathbf{L2a})_3]^{2+}$ and $[Fe(\mathbf{L4})_3]^{2+}$ cations in **4** and **5** adopt meridional arrangements, in which the $[FeN_6]$

Accepted Manuscript

This article is protected by copyright. All rights reserved.

chromophores only slightly deviate from perfect octahedrons according to SHAPE's scores (Table 1, entries 5-6).[32] The Fe-N bond lengths measured at 180 K are typical for a low-spin electronic configuration in *mer*-$[Fe(\mathbf{L2a})_3]^{2+}$ (1.96-2.03 Å), whereas the 10% expansion found in *mer*-$[Fe(\mathbf{L4})_3]^{2+}$ (2.14-2.26 Å, Table 1) is diagnostic for alternative high-spin configuration in the latter complex.[2]-[4]

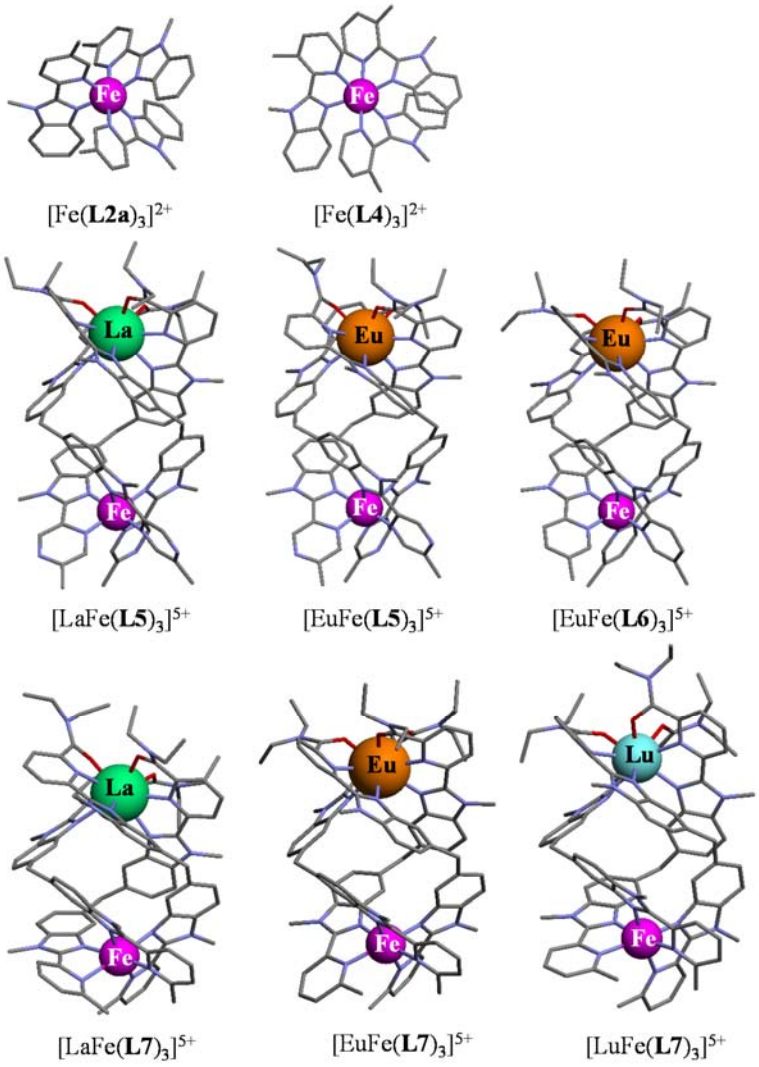

Figure 2. Molecular structures of the Fe^{II}-containing cations in the crystal structures of $[Fe(\mathbf{L2a})_3](PF_6)_2$ (**4**), $[Fe(\mathbf{L4})_3](ClO_4)_2{\cdot}CH_3CN$ (**5**) $[LaFe(\mathbf{L5})_3](ClO_4)_5{\cdot}5CH_3CN$ (**6**), $[EuFe(\mathbf{L5})_3](ClO_4)_5{\cdot}6CH_3CN$ (**7**), $[EuFe(\mathbf{L6})_3](CF_3SO_3)_5{\cdot}2.5CH_3CN{\cdot}(CH_3)_3C(OCH_3)$ (**8**), $\{[LaFe(\mathbf{L7})_3](ClO_4)_5\}_2{\cdot}6CH_3CN{\cdot}1.5H_2O$ (**9**), $\{[EuFe(\mathbf{L7})_3](CF_3SO_3)_5\}_2{\cdot}4CH_3CN{\cdot}3(CH_3)_3C(OCH_3)$ (**10**) and $[LuFe(\mathbf{L7})_3](CF_3SO_3)_5{\cdot}2CH_3CN$ (**11**)

Accepted Manuscript

This article is protected by copyright. All rights reserved.

Table 1. Structural data for the six-coordinate metallic (M = Fe^{II} or Zn^{II}) centers in complexes **4-11** in the solid state at 180 K.

Complexes	$[Zn(\mathbf{L2a})_3]^{2+}$	$[Fe(\mathbf{L2a})_3]^{2+}$	$[Fe(\mathbf{L4})_3]^{2+}$	$[EuZn(\mathbf{L5})_3]^{5+}$	$[LaFe(\mathbf{L5})_3]^{5+}$	$[EuFe(\mathbf{L5})_3]^{5+}$
$d_{M–N(bz)}$ /Å [a]	2.11(2)	1.96(1)	2.14(2)	2.09(3)	1.979(8)	1.973(9)
$d_{M–N(py/pz)}$ /Å [a]	2.24(4)	2.04(3)	2.26(5)	2.26(7)	1.98(1)	1.970(8)
α /° [b]	12(9)	11(3)	41.1(2)	17(7)	9(6)	8(2)
β /° [c]	87(2)	88.3(4)	76(5)	88(1)	85.5(5)	87(2)
Octahedron [d]	1.66	0.829	1.957	1.61	0.71	0.68
Trig. prism [d]	13.11	14.064	14.922	13.12	15.29	14.96
$d_{M–Ln}$ /Å [e]	-	-	-	8.92	9.19	9.17
Reference	[15]	This work	This work	[15]	This work	This work
Complexes	$[EuZn(\mathbf{L6})_3]^{5+}$	$[LaFe(\mathbf{L6})_3]^{5+}$	$[EuFe(\mathbf{L6})_3]^{5+}$	$[LaFe(\mathbf{L7})_3]^{5+}$	$[EuFe(\mathbf{L7})_3]^{5+}$	$[LuFe(\mathbf{L7})_3]^{5+}$
$d_{M–N(bz)}$ /Å [a]	2.05(6)	1.95(3)	1.968(5)	2.14(3)	2.13(2)	2.13(2)
$d_{M–N(py)}$ /Å [a]	2.3(2)	2.00(4)	1.988(4)	2.33(7)	2.34(7)	2.33(7)
α /° [b]	23(16)	9(4)	10.(2)	30(4)	23(11)	19(15)
β /° [c]	81(8)	86(2)	85(1)	76(4)	80(3)	80(5)
Octahedron [d]	1.88	0.91	0.75	3.0(4) [f]	2.7(2) [f]	2.79
Trig. prism [d]	14.40	15.07	15.54	14.9(9) [f]	14.3(7) [f]	13.53
$d_{M–Ln}$ /Å [e]	8.96	9.03	9.14	8.5(3) [f]	9.0(2)[f]	8.94
Reference	[18a]	[18b]	This work	This work	This work	This work

[a] Bz = benzimidazole, py = pyridine, pz = pyrazine. [b] Interannular intraligand angle. [c] Interchelate angle. [d] SHAPE's score for comparison with perfect octahedrons and trigonal prisms. [f] Average for the two independent complexes in the asymmetric unit.

Accepted Manuscript

This article is protected by copyright. All rights reserved.

The origin of these different spin states can be traced back to the considerable ligand-field splitting produced by heterocyclic nitrogen atoms, which favors low-spin configurations as found in *mer*-[Fe(**L2a**)$_3$]$^{2+}$. However, sterical constraints induced by the 3-methyl substituents in *mer*-[Fe(**L4**)$_3$]$^{2+}$ prevent coplanarity within the didentate polyaromatic rings (interannular angle α = 41° in *mer*-[Fe(**L4**)$_3$]$^{2+}$ compared with α = 11° in *mer*-[Fe(**L2a**)$_3$]$^{2+}$, Table 1). This reduces the ligand-field strength to such an extent that high-spin configuration becomes more stable in *mer*-[Fe(**L4**)$_3$]$^{2+}$.[7] Unfortunately, we were not able to isolate monocrystals of the facial isomers in the solid state for mononuclear complexes, but stoichiometric mixing of segmental ligands **L5**-**L7** (3.0 eq) with M(CF_3SO_3)$_2$ (M = Fe, Zn; 1.0 eq) and Ln(CF_3SO_3)$_3$ (Ln = La, Eu, Lu; 1.0 eq) in dichloromethane/acetonitrile followed by slow diffusion of volatile ether provided fair yields (68-93%) of microcrystalline [LnM(**L*k***)$_3$](CF_3SO_3)$_5$ complexes (Table S2), among which monocrystals suitable for X-ray crystal structure analyses could be obtained after a second crystallization (sometimes in presence of (^{n}Bu)$_4$NClO_4) for [LaFe(**L5**)$_3$](ClO_4)$_5$·5CH_3CN (**6**), [EuFe(**L5**)$_3$](ClO_4)$_5$·6CH_3CN (**7**), [EuFe(**L6**)$_3$](CF_3SO_3)$_5$·2.5CH_3CN·(CH_3)$_3$C(OCH_3) (**8**), {[LaFe(**L7**)$_3$](ClO_4)$_5$}$_2$·6CH_3CN·1.5H_2O (**9**), {[EuFe(**L7**)$_3$](CF_3SO_3)$_5$}$_2$·4CH_3CN·3(CH_3)$_3$C(OCH_3) (**10**) and [LuFe(**L7**)$_3$](CF_3SO_3)$_5$·2CH_3CN (**11**) (Figure 2 bottom, Tables S5-S10 and Figures S3-S8). As previously reported for [EuZn(**L5**)$_3$]$^{5+}$,[15] [EuZn(**L6**)$_3$]$^{5+}$ [18a] and [LaFe(**L6**)$_3$]$^{5+}$,[18b] the three helical strands adopt a head-to-head-to-head (*HHH*) arrangement[33] compatible with the formation of purely facial organization of the three didentate binding units around Fe^{II} or Zn^{II} (Figure 2 bottom). The intramolecular intermetallic distance (average $d_{M\text{-}Ln}$ = 9.0(2) Å) is roughly insensitive to the choice of the metals and to the nature of the terminal six-membered rings (substituted pyridine in **L6** and **L7** or pyrazine in **L5**). The Ln-O and Ln-N distances follow the expected lanthanide contraction along the La > Eu > Lu series (Figure 3 and Table S11 in the Supporting Information).[34] On the contrary, the Fe-N distances in a given helicate are insensitive to the size of the various capping trivalent lanthanide cations (Figure 3), a trend in line with the lack of measurable constraints induced by the flexible non-covalent lanthanide tripod.[16] In agreement with the analogous mononuclear *mer*-

Accepted Manuscript

This article is protected by copyright. All rights reserved.

[Fe(**L2a**)$_3$]$^{2+}$ complex, the Fe-N distances (1.95-2.00 Å, Table 1) observed at 180 K for *HHH*-[LnFe(**L6**)$_3$]$^{5+}$ points to low-spin configuration, this whatever the meridional (mononuclear) or facial (dinuclear helicate) arrangements of the three (5-methylpyridin-2-yl)-benzimidazole binding units around Fe^{II}. Extension to (5-methylpyrazin-2-yl)-benzimidazoles in [LnFe(**L5**)$_3$]$^{5+}$ gives similar Fe-N distances (1.97-1.98 Å) and low-spin characteristics. On the contrary, constrained (6-methylpyridine-2-yl)-benzimidazole units in [LnFe(**L7**)$_3$]$^{5+}$ lead to high-spin configurations at 180 K with larger Fe-N distances (2.13-2.34 Å, Table 1) as previously discussed for *mer*-[Fe(**L4**)$_3$]$^{2+}$.

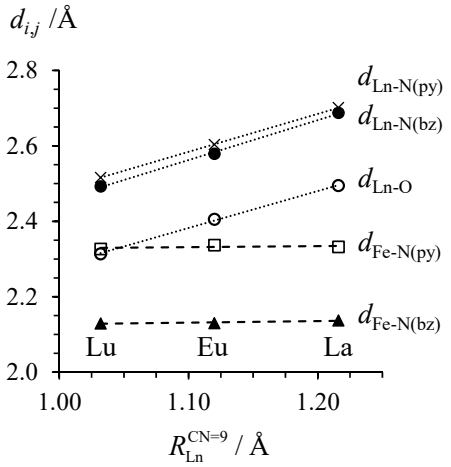

Figure 3. Interatomic distances d_{Ln-O}, d_{Ln-N} and d_{Fe-N} measured for the *HHH*-[LnFe(**L7**)$_3$]$^{5+}$ cations in the crystal structures of **9-11** at 180 K (py = pyridine, bz = benzimidazole; $R_{Ln}^{CN=9}$ = nine-coordinate lanthanide ionic radius) .

The molar magnetic susceptibilities (χ_M) corrected for diamagnetism and for Fe^{III} contamination recorded at variable temperature for solid state samples confirm the spin states deduced by X-ray diffraction studies at 180 K with negligible $0.00 \le C_{ls} \le 0.8$ cm^3·K·mol^{-1} Curie constants for the low-spin Fe^{II} complexes with ligands **L1**, **L2**, **L5** and **L6** at this temperature (Figure 4; $C = \chi_M T = \left(N\beta^2/3k_B\right) g^2 S\left(S+1\right) \simeq \left(g^2/8\right) S\left(S+1\right)$, where N is Avagadro number, β is Bohr magneton, k_B is Boltzmann constant, g = 2 is Landé factor, S is the total spin quantum number).[35] On the other hand, the homoleptic tris-didentate Fe^{II} complexes with sterically demanding ligands **L4** and **L7** possess significant Curie constants ($3.5 \le C_{ls} \le 3.8$ cm^3·K·mol^{-1}, Figure 4) diagnostic for high-spin Fe^{II} (S = 2) configuration at this temperature.[36] Upon warming the samples, $\chi_M \cdot T$ for complexes

Accepted Manuscript

This article is protected by copyright. All rights reserved.

with ligands **L4** and **L7** do not significantly change, a trend in line with the existence of pure high-spin configuration. The abrupt decrease of $\chi_M \cdot T$ at very low temperature is diagnostic for the existence of axial zero-field splittings fitted to D = 1.37 cm^{-1} and g = 2.26 for [Fe(**L4**)$_3$](PF$_6$)$_2$.[37]

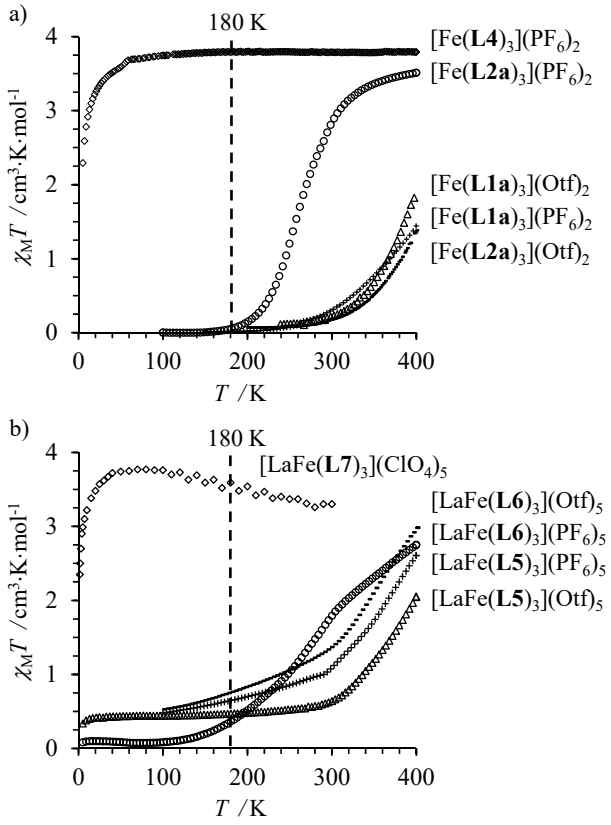

Figure 4. $\chi_M \cdot T$ versus T plot of the molar magnetic susceptibilities (χ_M) corrected for diamagnetism and for Fe^{III} contamination recorded for a) mononuclear and b) dinuclear homoleptic tris-diimine Fe^{II} complexes (solid state, Otf$^-$ = $CF_3SO_3^-$). The temperature at which the X-ray crystal structures have been measured is highlighted (180 K).

For complexes with ligands **L1**, **L2**, **L5** and **L6**, $\chi_M \cdot T$ values smoothly increase with temperature, a behavior diagnostic for the operation of thermodynamic temperature-driven spin state equilibria. All curves can be satisfyingly fitted with standard Eq. (2), where C_{ls}, C_{hs} and $C_{Fe(III)}$ correspond to the Curie constants of the incriminated electronic configurations and TIP_{hs} and TIP_{hs} refer to the temperature independent paramagnetic contributions, see next section.[2d],[38] The mole fraction of high-spin complexes (x_{hs}) can be further deduced with Eq. (3) when one takes into account the mass balance $x_{ls} + x_{hs} + x_{Fe(III)} = 1$.

Accepted Manuscript

This article is protected by copyright. All rights reserved.

$$\chi_M T = x_{hs} \cdot \left(C_{hs} + T \cdot TIP_{hs}\right) + x_{ls} \cdot \left(C_{ls} + T \cdot TIP_{ls}\right) + x_{Fe(III)} \cdot C_{Fe(III)} \quad (2)$$

$$x_{hs} = \frac{\chi_M T - T \cdot TIP_{ls} - C_{ls} + x_{Fe(III)} \cdot \left(C_{ls} - C_{Fe(III)} + T \cdot TIP_{ls}\right)}{C_{hs} - C_{ls} + T \cdot \left(TIP_{hs} - TIP_{ls}\right)} \quad (3)$$

In the solid state, the spin transition leads to 25 to 100% of high-spin Fe^{II} at the highest accessible temperature (400 K, Figure S9, Supporting information), but no rational correlation can be drawn between the local molecular structures (*mer*/*fac* isomerism or pyridine *versus* pyrazine donor groups) and the SCO properties. Major variations are observed upon exchange of non-coordinated (*i*. *e*. ionic) counter-anions, which indicates that intermolecular contributions and packing effects largely dominate local effects in the solid state. The record of heating/cooling cycles shows no evidence of cooperativity for the SCO processes in the solid state. A thorough study of the temperature dependence of the volume of the crystallographic unit cell of $[Fe(\mathbf{L2a})_3](PF_6)_2$ (**4**) confirms the operation of a complete smooth spin transition for this complex in the 200-350 K range with an unit cell expansion of 31.2(6) Å (Appendix 1).

Solution SCO processes for Fe(II) complexes with ligands L1-L4: a molecular approach to spin-state equilibria. In solution, the minor second-sphere interactions between the solvent molecules and six-coordinate homoleptic tris-diimine $[Fe(\mathbf{L}\boldsymbol{k})_3]^{2+}$ cations are expected to produce only minor energy contributions, thus allowing the deciphering of chemically-programmable structural effects. Following the procedure previously detailed for analogous $[Zn(\mathbf{L}\boldsymbol{k})_3]^{2+}$ with the didentate ligands **L1a**, **L1b**, **L2a** and **L2b**,[15] spectrophotometric titrations of these ligands with $Fe(CF_3SO_3)_2$ in dry acetonitrile (Figure 5a,b and Figures S10a,b-S12a,b) show the successive formation of the expected three absorbing complexes $[Fe(\mathbf{L}\boldsymbol{k})_n]^{2+}$ (n = 3, 2, 1) as ascertained by their independent eigenvectors found in the factor analyses (Figures 5c and S10c-S12c)[21] and their satisfying re-constructed absorption spectra (Figures 5d and S10d-S12d).

Accepted Manuscript

This article is protected by copyright. All rights reserved.

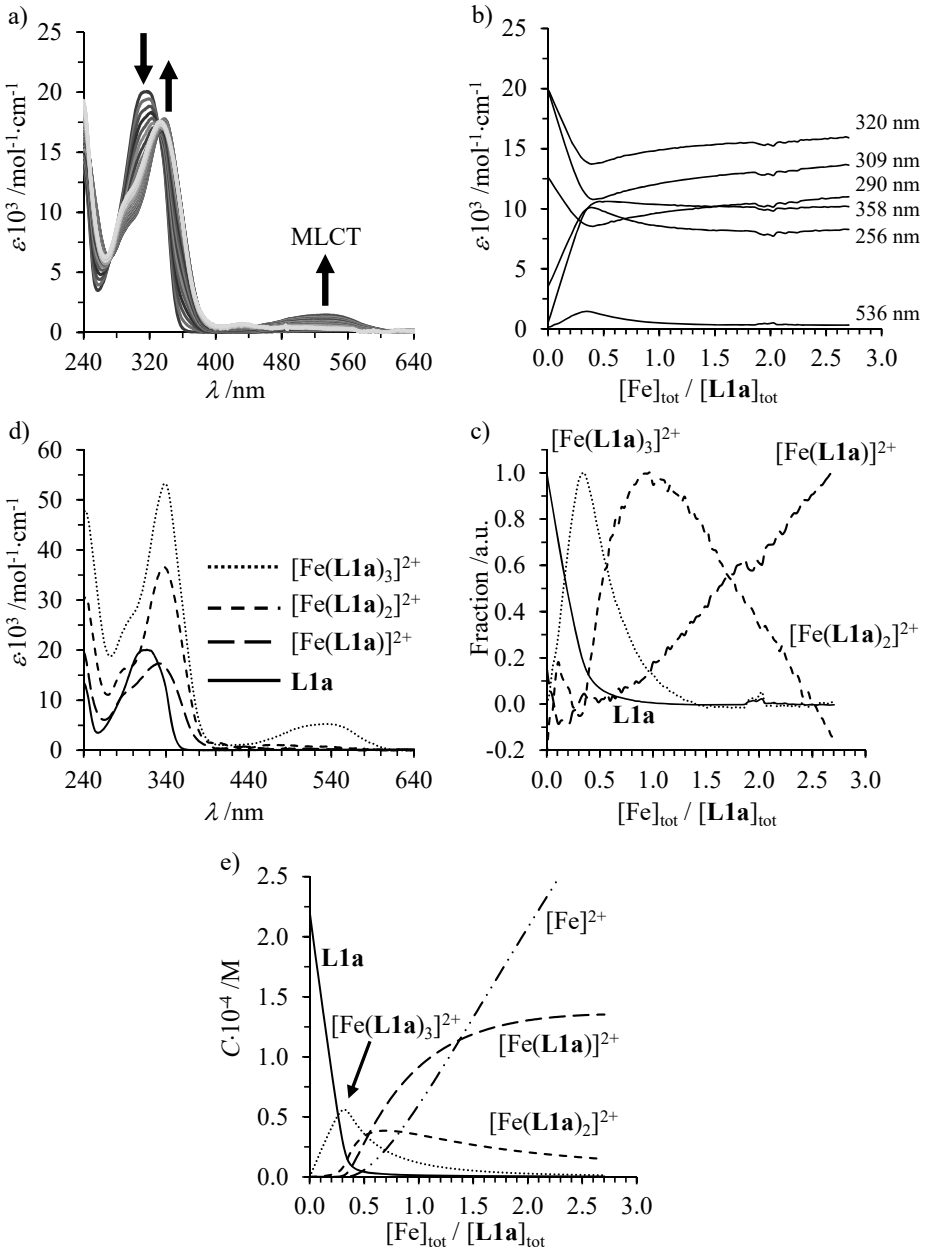

Figure 5. a) Variation of absorption spectra and b) corresponding variation of observed molar extinctions at different wavelengths recorded for the spectrophotometric titration of **L1a** with $Fe(CF_3SO_3)_2$ (total ligand concentration: $2.3 \cdot 10^{-4}$ mol·dm^{-3} in acetonitrile, 298 K). c) Evolving factor analysis using four absorbing eigenvectors,[21] d) re-constructed individual electronic absorption spectra[22] and e) associated speciation.[39]

Beyond (i) the diagnostic 2000 cm^{-1} red-shift of the ligand-centered $\pi^* \leftarrow \pi$ transition observed upon complexation to Fe^{II} (Figure 5a,d and S10a,d-S12a,d)[40] and (ii) the stepwise increase of the molar absorption coefficients along the $[Fe(\mathbf{L}\boldsymbol{k})]^{2+} \rightarrow [Fe(\mathbf{L}\boldsymbol{k})_2]^{2+} \rightarrow [Fe(\mathbf{L}\boldsymbol{k})_3]^{2+}$ series (Figure 5d and S10d-S12d), the absorption spectrum of $[Fe(\mathbf{L}\boldsymbol{k})_3]^{2+}$ displays a supplementary broad absorption band

Accepted Manuscript

This article is protected by copyright. All rights reserved.

covering the visible domain (440-600 nm), which can be unambiguously assigned to the **L*k*** ←Fe^{II} metal-to-ligand charge transfer transition (MLCT) occurring in the low-spin iron(II) complex.[41] Non-linear least-square fits[22] of the spectrophotometric data to equilibria (4)-(6) provided the macroscopic cumulative formation constants gathered in Table S12 together with speciation curves (Figures 5e and S10e-S12e),[39] which indicate that the target complexes $[Fe(\mathbf{L}\boldsymbol{k})_3]^{2+}$ are quantitatively formed for 1:3 stoichiometric ratio at sub-millimolar concentrations.

$$Fe^{2+} + \mathbf{L}\boldsymbol{k} \rightleftharpoons [Fe\mathbf{L}\boldsymbol{k}]^{2+} \qquad \beta_{1,1}^{Fe,\mathbf{L}\boldsymbol{k}} \qquad (4)$$

$$Fe^{2+} + 2\,\mathbf{L}\boldsymbol{k} \rightleftharpoons [Fe(\mathbf{L}\boldsymbol{k})_2]^{2+} \qquad \beta_{1,2}^{Fe,\mathbf{L}\boldsymbol{k}} \qquad (5)$$

$$Fe^{2+} + 3\,\mathbf{L}\boldsymbol{k} \rightleftharpoons [Fe(\mathbf{L}\boldsymbol{k})_3]^{2+} \qquad \beta_{1,3}^{Fe,\mathbf{L}\boldsymbol{k}} \qquad (6)$$

Application of the site-binding model summarized in Eqs (7)-(9)[15] dissects the free energy changes accompanying the complexation processes into (1) a pure entropic contribution produced by the change in rotational entropies accompanying the transformation of the reactants into products, a parameter often referred to as the statistical factor,[42] (2) a simple intermolecular affinity $f^{Fe,\mathbf{L}\boldsymbol{k}}$ between the didentate ligand and the entering Fe^{II} cation (including the change in solvation) and (3) allosteric cooperativity factors $u_{i,j}^{\mathbf{L}\boldsymbol{k},\mathbf{L}\boldsymbol{k}}$ measuring the extra energy cost ($u_{i,j}^{\mathbf{L}\boldsymbol{k},\mathbf{L}\boldsymbol{k}} < 1$), respectively energy benefit ($u_{i,j}^{\mathbf{L}\boldsymbol{k},\mathbf{L}\boldsymbol{k}} > 1$) produced by an already bound ligand for the connection of the next one around Fe^{II}.[43] Since different microspecies contribute to the $[Fe(\mathbf{L}\boldsymbol{k})_2]^{2+}$ and $[Fe(\mathbf{L}\boldsymbol{k})_3]^{2+}$ macrospecies in solution (Figure S13),[15] various intramolecular interligand cooperativity factors $u_{i,j}^{\mathbf{L}\boldsymbol{k},\mathbf{L}\boldsymbol{k}}$ should be considered (Eqs (7)-(9)).

$$\beta_{1,1}^{Fe,\mathbf{L}\boldsymbol{k}} = 24 f^{Fe,\mathbf{L}\boldsymbol{k}} \qquad (7)$$

$$\beta_{1,2}^{Fe,\mathbf{L}\boldsymbol{k}} = 12\left(f^{Fe,\mathbf{L}\boldsymbol{k}}\right)^2\left(u_{trans,fac}^{\mathbf{L}\boldsymbol{k},\mathbf{L}\boldsymbol{k}} + u_{trans,mer}^{\mathbf{L}\boldsymbol{k},\mathbf{L}\boldsymbol{k}} + 4u_{cis,fac}^{\mathbf{L}\boldsymbol{k},\mathbf{L}\boldsymbol{k}} + 4u_{cis,mer}^{\mathbf{L}\boldsymbol{k},\mathbf{L}\boldsymbol{k}}\right) \qquad (8)$$

$$\beta_{1,3}^{Fe,\mathbf{L}\boldsymbol{k}} = 16\left(f^{Fe,\mathbf{L}\boldsymbol{k}}\right)^3 u_{cis,fac}^{\mathbf{L}\boldsymbol{k},\mathbf{L}\boldsymbol{k}}\left[\left(u_{cis,fac}^{\mathbf{L}\boldsymbol{k},\mathbf{L}\boldsymbol{k}}\right)^2 + 3\left(u_{cis,mer}^{\mathbf{L}\boldsymbol{k},\mathbf{L}\boldsymbol{k}}\right)^2\right] \qquad (9)$$

Accepted Manuscript

This article is protected by copyright. All rights reserved.

With the only resort to the three macroscopic formation constants obtained by spectrophotometric titrations, one roughly assumes that $u_{cis,fac}^{\mathbf{L}k,\mathbf{L}k} = u_{cis,mer}^{\mathbf{L}k,\mathbf{L}k} = u_{trans,fac}^{\mathbf{L}k,\mathbf{L}k} = u_{trans,mer}^{\mathbf{L}k,\mathbf{L}k} = u^{\mathbf{L}k,\mathbf{L}k}$, and the multi-linear fits of the experimental $\beta_{1,1}^{\mathrm{Fe},\mathbf{L}k}$ to Eqs (7)-(9) gives the intrinsic metal-ligand affinities $\Delta G^{\mathrm{Fe},\mathbf{L}k} = -RT\ln\left(f^{\mathrm{Fe},\mathbf{L}k}\right)$ and allosteric interligand interactions $\Delta E_{i,j}^{\mathbf{L}k,\mathbf{L}k} = -RT\ln(u_{i,j}^{\mathbf{L}k,\mathbf{L}k})$ illustrated in Figure 6 and tabulated in Table S12.

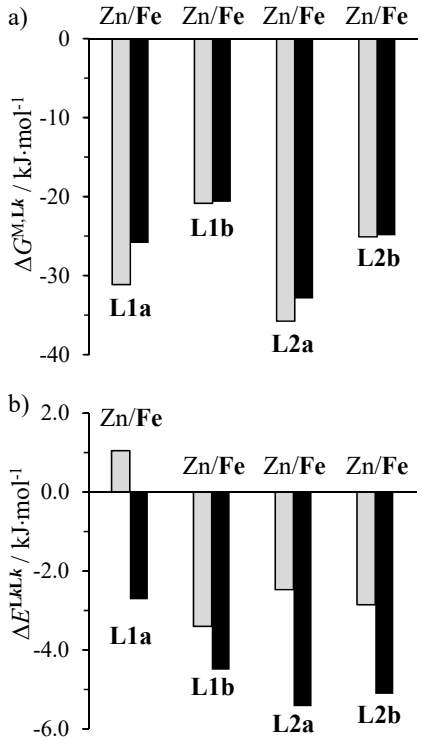

Figure 6. a) Intrinsic affinities $\Delta G^{\mathrm{M},\mathbf{L}k} = -RT\ln\left(f^{\mathrm{M},\mathbf{L}k}\right)$ and b) global interligand interactions $\Delta E^{\mathbf{L}k,\mathbf{L}k} = -RT\ln(u^{\mathbf{L}k,\mathbf{L}k})$ for the complexation of $M(CF_3SO_3)_2$ with ligands **L*k*** obtained by fitting equilibria (4)-(6) with the help of the site-binding model (Eqs (7-9); $u_{cis,fac}^{\mathbf{L}k,\mathbf{L}k} = u_{cis,mer}^{\mathbf{L}k,\mathbf{L}k} = u_{trans,fac}^{\mathbf{L}k,\mathbf{L}k} = u_{trans,mer}^{\mathbf{L}k,\mathbf{L}k} = u^{\mathbf{L}k,\mathbf{L}k}$; acetonitrile at 298 K).

In line with the Irving-Williams series,[44] the affinities of ligands **L*k*** for Fe^{II} is marginally smaller than those with Zn^{II} (Figure 6a). The ethyl substituents connected to the benzimidazole units in **L1b** and **L2b** reduce the affinity for any entering metal by *circa* 10 kJ/mol because of the sterical constraints produced in the bound *cis*-*cis*-chelate conformation.[15] Remarkably, the recurrent global positive cooperativity accompanying the successive complexation of didentate ligands to Fe^{II} (-5 ≤

Accepted Manuscript

This article is protected by copyright. All rights reserved.

$\Delta E_{\mathrm{Fe}}^{\mathbf{L}\boldsymbol{k},\mathbf{L}\boldsymbol{k}} \leq$ -3 kJ/mol) is at least twice as large as that measured in the Zn(II) analogues (-2 $\leq \Delta E_{\mathrm{Zn}}^{\mathbf{L}\boldsymbol{k},\mathbf{L}\boldsymbol{k}} \leq$ 1 kJ/mol, Figure 6b). This trend is reminiscent of $\Delta E_{\mathrm{M}}^{\mathbf{bipy},\mathbf{bipy}}$ estimated with Eqs. (7)-(9) for $[\mathrm{M}(\mathbf{bipy})_n]^{2+}$ in water, where the minor values found for M = Zn, $\Delta E_{\mathrm{Zn}}^{\mathbf{bipy},\mathbf{bipy}}$ = -0.57(7) kJ/mol becomes much more negative in $[\mathrm{Fe}(\mathbf{bipy})_n]^{2+}$ ($\Delta E_{\mathrm{Fe}}^{\mathbf{bipy},\mathbf{bipy}}$ = -18(7) kJ/mol) because the coordination of a third ligand to high-spin $[\mathrm{Fe}(\mathbf{bipy})_2]^{2+}$ (possessing two anti-bonding electrons) gives low-spin $[\mathrm{Fe}(\mathbf{bipy})_3]^{2+}$ with no anti-bonding electron.[45] The less drastic effect observed in going from $[\mathrm{Fe}(\mathbf{L}\boldsymbol{k})_2]^{2+}$ and $[\mathrm{Fe}(\mathbf{L}\boldsymbol{k})_3]^{2+}$ can be tentatively assigned to the smaller ligand-field strength produced by **L1** or **L2**, compared with **bipy**, thus leading to spin-crossover $[\mathrm{Fe}(\mathbf{L}\boldsymbol{k})_3]^{2+}$ complexes instead of pure low-spin entities.

Since $\mathrm{Fe^{II}}$ complexes are kinetically less labile than their $\mathrm{Zn^{II}}$ analogues,[46] separated ^{1}H NMR signals for the microspecies *mer*-$[\mathrm{Fe}(\mathbf{L}\boldsymbol{k})_3]^{2+}$ and *fac*-$[\mathrm{Fe}(\mathbf{L}\boldsymbol{k})_3]^{2+}$ (**L*k*** = **L1a**, **L2a**; Figure S14) can be observed in the 233-293 K range (Figure S15), while coalescence due to fast exchange processes on the NMR time scale already occurs at 250 K for $\mathrm{Zn^{II}}$ analogues.[15] The integration of the ^{1}H NMR signals at variable temperatures gives $K_{mer\rightarrow fac}^{\mathrm{Fe},\mathbf{L}\boldsymbol{k}}$ (Eq. (10)), from which the enthalpic $\Delta H_{mer\rightarrow fac}^{\mathrm{Fe},\mathbf{L}\boldsymbol{k}}$ and entropic $\Delta S_{mer\rightarrow fac}^{\mathrm{Fe},\mathbf{L}\boldsymbol{k}}$ contributions are deduced with the help of van't Hoff plots (Table S13 and Figure S16).

$$mer\text{-}[\mathrm{Fe}(\mathbf{L}\boldsymbol{k})_3]^{2+} \rightleftharpoons fac\text{-}[\mathrm{Fe}(\mathbf{L}\boldsymbol{k})_3]^{2+} \qquad K_{mer\rightarrow fac}^{\mathrm{Fe},\mathbf{L}\boldsymbol{k}} \qquad (10)$$

In agreement with an identical analysis performed for $\mathrm{Zn^{II}}$ analogues, a weak, but non-negligible enthalpic driving force (-5 $\leq \Delta H_{mer\rightarrow fac}^{\mathrm{Fe},\mathbf{L}\boldsymbol{k}} \leq$ -3 kJ/mol) favors the formation of the facial isomers *fac*-$[\mathrm{Fe}(\mathbf{L}\boldsymbol{k})_3]^{2+}$, the signature of a weak thermodynamic *trans*-influence.[15] Specific solvation effects [15] produce negative entropic contributions (-17 $\leq \Delta S_{mer\rightarrow fac}^{\mathrm{Fe},\mathbf{L}\boldsymbol{k}} \leq$ -13 J/mol·K), which (i) exceed the expected statistical factor $\Delta S_{mer\rightarrow fac}^{\mathrm{Fe},\mathbf{L}\boldsymbol{k},\mathrm{stat}} = -R\ln(1/3)$ = -9.1 J/mol·K and (ii) oppose the enthalpic trend thus making *mer*-$[\mathrm{Fe}(\mathbf{L}\boldsymbol{k})_3]^{2+}$ the major isomer in acetonitrile at room temperature. Application of the site-binding model to Equilibrium (10) yields Eq. (11),[43] which can be combined with Eqs (7)-(9) to

Accepted Manuscript

This article is protected by copyright. All rights reserved.

partition the rough cooperativity factors $u^{\mathbf{Lk},\mathbf{Lk}}$ into $u^{\mathbf{Lk},\mathbf{Lk}}_{trans,fac} = u^{\mathbf{Lk},\mathbf{Lk}}_{trans,mer} = u^{\mathbf{Lk},\mathbf{Lk}}_{trans}$, $u^{\mathbf{Lk},\mathbf{Lk}}_{cis,fac}$ and $u^{\mathbf{Lk},\mathbf{Lk}}_{cis,mer}$ (Table S12).

$$K^{\mathrm{Fe},\mathbf{Lk}}_{mer\rightarrow fac} = \frac{\beta^{\mathrm{Fe},\mathbf{Lk}}_{1,3,fac}}{\beta^{\mathrm{Fe},\mathbf{Lk}}_{1,3,mer}} = \frac{1}{3}\cdot\left(\frac{u^{\mathbf{Lk},\mathbf{Lk}}_{cis,fac}}{u^{\mathbf{Lk},\mathbf{Lk}}_{cis,mer}}\right)^2 \quad (11)$$

With this thermodynamic toolkit in hand, we are able to catch the meridional/facial speciation of $[Fe(\mathbf{Lk})_3]^{2+}$ at any temperature in acetonitrile solution (Figure S17), a pre-requisite for assigning specific magnetic SCO properties to each isomer. Moreover, the stability constants collected for Fe^{II} and Zn^{II} (Table S12) are strong support for assuming that the closely related homoleptic pseudo-octahedral $[Ni(\mathbf{Lk})_3]^{2+}$ complexes (existing as mixtures of *mer*/*fac* isomers) are quantitatively formed in acetonitrile at 0.1 M, where well-resolved absorption spectra can be recorded for the $Ni(^3T_{2g}\leftarrow{}^3A_{2g})$, $Ni(^3T_{1g}\leftarrow{}^3A_{2g})$ and $Ni(^1E_g\leftarrow{}^3A_{2g})$ d-d transitions (the symmetry labels assume O_h symmetry, Figure S18). Non-linear least-square fits of the experimental energies at the maximum of the absorption bands (Table S14) with the ligand-field Eqs (12-15) pertinent to octahedral d^8 systems[47],[48] give the ligand-field strengths Δ_{oct} and Racah parameters B and C collected in Table 2.

$$E\left(^3A_{2g}\right) = 0 \quad (12)$$

$$E\left(^1E_g\right) = 8B + 2C - \frac{6B^2}{\Delta_{oct}} \quad (13)$$

$$E\left(^3T_{2g}\right) = \Delta_{oct} \quad (14)$$

$$E\left(^3T_{1g}\right) = 1.5\Delta_{oct} + 7.5B - 0.5\sqrt{225B^2 + \Delta_{oct}{}^2 - 18\Delta_{oct}B} \quad (15)$$

This well-established procedure overcomes the difficult detection of weak d-d transitions masked by intense charge transfer band found in Fe^{II} complexes.[49] Ligand-field strength in the $11200 \leq \Delta_{oct}(Ni^{II}) \leq 12400$ cm^{-1} range corresponds to the accepted limits for inducing accessible SCO behavior in Fe^{II} analogues,[2a] but it may induce some uncertainties for the calculation of the exact values of $\Delta_{oct}(Ni^{II})$ due to the mixing of spin-allowed $^3T_{2g}\leftarrow{}^3A_{2g}$ with the spin-forbidden $^1E_g\leftarrow{}^3A_{2g}$.[50] Further refinements using the improved equation proposed by Hart et al[50] provide $\Delta_{oct}(Ni(\mathbf{L1a})_3) = 11730$

Accepted Manuscript

This article is protected by copyright. All rights reserved.

cm^{-1}, $\Delta_{oct}(Ni(\mathbf{L1b})_3)$ = 11880 cm^{-1}, $\Delta_{oct}(Ni(\mathbf{L2a})_3)$ = 11680 cm^{-1} and $\Delta_{oct}(Ni(\mathbf{L2b})_3)$ = 11780 cm^{-1}, which deviate by less than 2% of those estimated in absence of mixing (eq. 14, column 2 in Table 2).

Table 2. Ligand-field strengths (Δ_{oct}), Racah parameters *B* et *C* and nephelauxetic parameters β for homoleptic $[Ni(\mathbf{L}\boldsymbol{k})_3]^{2+}$ complexes (acetonitrile, 293 K).

complexes	Δ_{oct} /cm^{-1}	*B* /cm^{-1}	*C* /cm^{-1}	*C*/*B*	Δ_{oct}/B	β [a]	Reference
$[Ni(\mathbf{bipy})_3]^{2+}$	12699	741	2801	3.78	17.1	0.71	This work
$[Ni(\mathbf{L1a})_3]^{2+}$	11476	866	3149	3.64	13.3	0.83	This work
$[Ni(\mathbf{L1b})_3]^{2+}$	11628	878	3072	3.50	13.2	0.84	This work
$[Ni(\mathbf{L2a})_3]^{2+}$	11423	889	3096	3.48	12.9	0.85	This work
$[Ni(\mathbf{L2b})_3]^{2+}$	11567	882	3067	3.48	13.1	0.85	This work
$[Ni(\mathbf{L3})_3]^{2+}$	9644	994	2614	2.63	9.7	0.95	This work
$[Ni(\mathbf{L4})_3]^{2+}$	10681	918	2800	3.05	11.6	0.88	This work
$[Ni(CH_3CN)_6]^{2+}$	10100	864	3708	4.29	11.7	0.83	This work
$[Ni(NH_3)_6]^{2+}$	10730	830	[b]	[b]	12.9	0.80	[48]
$[Ni(H_2O)_6]^{2+}$	8580	929	[b]	[b]	9.2	0.89	[48]

[a] Nephelauxetic parameter $\beta = B/B^o$ with B^o = 1042 cm^{-1} for free Ni^{2+}.[6b] [b] Not computed in reference [48].

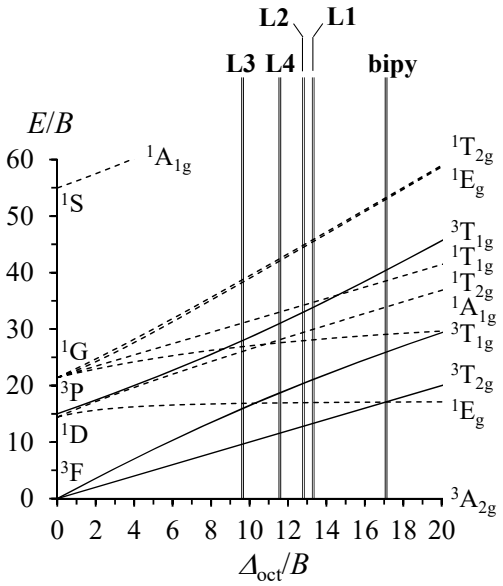

Figure 7. *Tanabe-Sugano* diagram built for the d^8 electronic configuration (C^o/B^o = 4.71 taken for the free Ni^{2+} ion)[8] highlighting the Δ_{oct}/B ratio observed for $[Ni(\mathbf{L}\boldsymbol{k})_3]^{2+}$ in acetonitrile solution.[8]

Accepted Manuscript

This article is protected by copyright. All rights reserved.

Neglecting this minor effect, Table 2 predicts that $[Fe(\mathbf{L1})_3]^{2+}$ and $[Fe(\mathbf{L2})_3]^{2+}$ display SCO behavior in solution, whereas $[Fe(\mathbf{L3})_3]^{2+}$ and $[Fe(\mathbf{L4})_3]^{2+}$ adopt pure high-spin state. Furthermore, the slightly larger nephelauxetic effect produced by the remarkable π-accepting properties of terminal pyrazine groups in **L1**[51] shifts Δ_{oct}/B toward high values. The associated SCO behavior is thus expected to occur at higher temperature for $[Fe(\mathbf{L1})_3]^{2+}$ than for $[Fe(\mathbf{L2})_3]^{2+}$ (Figure 7), a trend previously documented for related replacements of pyridine rings with pyrazine analogues.[52] Since the NMR spectra recorded for $[Fe(\mathbf{L}\boldsymbol{k})_3]^{2+}$ in acetonitrile are complicated by *mer*/*fac* isomerization and by paramagnetic line broadening (Figure S15), we gave up chemical shifts techniques[53] and preferred to use the Evans' method[24],[27] adapted for systems with non-negligible diamagnetic contributions (Eq. 16).[28] The corrected magnetic susceptibilities χ_M are obtained from the balance between the shifts in frequency of the paramagnetic sample $\Delta\nu^{para}$ (Hz) with respect to *tert*-butanol taken as the reference (measured for the $[Fe(\mathbf{L}\boldsymbol{k})_3]^{2+}$ complex of molecular mass M^{para} ($g\cdot mol^{-1}$) and at concentration m^{para} ($g\cdot cm^3$)) and that of the diamagnetic analogue $\Delta\nu^{dia}$ (measured for $[Zn(\mathbf{L}\boldsymbol{k})_3]^{2+}$ of molecular mass M^{dia} at concentration m^{dia}). In Eq (16), ν_0 stands for the operating frequency of the NMR spectrometer in Hz and $S_f = 4\pi/3$ is the shape factor of the superconducting magnet.[28]

$$\chi_M = \frac{1}{\nu_0 S_f}\left(\frac{\Delta\nu^{para} M^{para}}{m^{para}} - \frac{\Delta\nu^{dia} M^{dia}}{m^{dia}}\right) \qquad (16)$$

Plots of $\chi_M T$ products versus T collected in Figure 8 show pure high-spin character for $[Fe(\mathbf{L3})_3]^{2+}$ and $[Fe(\mathbf{L4})_3]^{2+}$ and pure low-spin character for $[Fe(\mathbf{bipy})_3]^{2+}$ in complete agreement with previous solid state measurements (Figure 4a).[45b],[54] Non-linear least-squares fits using Eq. (2) provide Curie constants of $3.41 \le C_{hs} \le 3.44$ $cm^3\cdot K\cdot mol^{-1}$ typical for high-spin $[Fe(\mathbf{L3})_3]^{2+}$ and $[Fe(\mathbf{L4})_3]^{2+}$ (expected range 3.13-3.65 $cm^3\cdot K\cdot mol^{-1}$)[55] and $C_{ls} = 0.00(8)$ $cm^3\cdot K\cdot mol^{-1}$ typical for low-spin $[Fe(\mathbf{bipy})_3]^{2+}$. The contributions of temperature-independent paramagnetism are opposite, but in the same range as the diamagnetic response for $[Fe(\mathbf{L4})_3]^{2+}$ ($TIP_{hs} = 358(57)\cdot10^{-6}$ $cm^3\cdot K\cdot mol^{-1}$) and for $[Fe(\mathbf{bipy})_3]^{2+}$ (TIP_{ls} = $351(55)\cdot10^{-6}$ $cm^3\cdot K\cdot mol^{-1}$, Table 3). Using these values for pure high-spin, respectively pure low

Accepted Manuscript

This article is protected by copyright. All rights reserved.

spin configurations allows the non-linear least-square fit of the $\chi_M T$ versus T curves recorded for the spin crossover complexes $[Fe(\mathbf{L1})_3]^{2+}$ and $[Fe(\mathbf{L2})_3]^{2+}$ with the help of Eqs (1)-(2) (see Appendix 2 for details). In solution, the estimated enthalpic (ΔH_{SCO}) and entropic (ΔS_{SCO}) contributions to the spin state equilibria (Table 3) are essentially independent from the choice of the counter anions (Table 3).[56] However, the replacement of pyrazine rings in $[Fe(\mathbf{L1})_3]^{2+}$ with pyridine rings in $[Fe(\mathbf{L2})_3]^{2+}$ significantly decreases ΔH_{SCO}, while ΔS_{SCO} is poorly affected. As a result, the 'transition' temperature $T_{1/2}$ at which $x_{ls} = x_{hs} = 0.5$ is shifted by 40 K toward high temperature for $[Fe(\mathbf{L1})_3]^{2+}$ (Figure 8 and Table 3), a trend in line with stronger Fe-N interactions and a larger Δ_{oct}/B parameter found for this ligand (larger π-backbonding, *vide infra*).

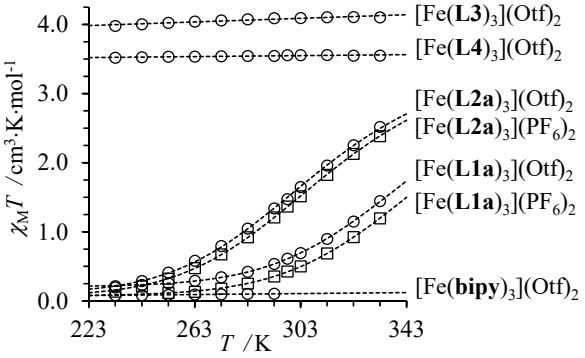

Figure 8. Corrected $\chi_M T$ products plotted as a function of the temperature for 0.01 M solution of $[Fe(\mathbf{L}k)_3](CF_3SO_3)_2$ (discs) or $[Fe(\mathbf{L}k)_3](PF_6)_2$ (squares) in CD_3CN. The dotted traces correspond to non-linear least-square fits obtained with Eqs (1)-(2) and using the parameters gathered in Table 3.

Two additional points merit to be highlighted here. Firstly, an especially large $TIP_{hs} = 1321(88)\cdot10^{-6}$ $cm^3\cdot K\cdot mol^{-1}$ is found for high-spin $[Fe(\mathbf{L3})_3]^{2+}$ because the sterically hindered approach of the 6-methyl-pyridine rings produces very weak ligand-field (Table 2) and, consequently, large second-order Zeeman contributions via the spin-orbit coupling mechanism.[35] Secondly, the thermodynamic parameters ΔH_{SCO} and ΔS_{SCO} recorded for $[Fe(\mathbf{L1})_3]^{2+}$ and $[Fe(\mathbf{L2})_3]^{2+}$ refer to average values characterizing a mixture of temperature-dependent *mer*/*fac* isomers, probably both displaying specific and different SCO behaviors (see next section).

Accepted Manuscript

This article is protected by copyright. All rights reserved.

Solution SCO processes for LnFe(II) helicates with ligands L5-L7: deciphering meridional/facial contributions. Stoichiometric mixing of segmental ligands **L5**-**L7** (3 eq.) with $M(CF_3SO_3)_2$ (1 eq, M = Fe^{II}, Zn^{II}) and $Ln(CF_3SO_3)_3$ (1 eq, Ln = La^{III}, Eu^{III}) in acetonitrile at millimolar concentrations quantitatively form C_3-symmetrical *HHH*-[LnM(**L*k***)$_3$)]$^{5+}$ triple-stranded helicates as ascertained by ESI-MS data (qualitative speciation, Figure S19 and Table S15) and ^{1}H NMR spectra (quantitative speciation, Figures S20-S24). These results corroborate detailed solution studies previously reported for [EuZn(**L5**)$_3$]$^{5+}$ [15] and [LnM(**L6**)$_3$]$^{5+}$,[18] and they unambiguously establish that the divalent d-block Fe^{II} or Zn^{II} cations are facially coordinated by three unsymmetrical diimine units in these C_3-symmetrical dinuclear complexes in solution, as depicted in their crystal structures (Figure 2). The associated corrected magnetic susceptibilities χ_M, recorded using Evans' method in CD_3CN (Eq. (16)) and plotted as $\chi_M T$ versus T curves (Figure 9), show pure high-spin behavior for [LaFe(**L7**)$_3$]$^{5+}$ with the constrained ligand **L7**. The magnetic behavior of the latter complex provides reliable estimates for C_{hs} = 3.44(4) cm^3·K·mol^{-1} and TIP_{hs} = 310(15)·10^{-6} cm^3·mol^{-1} using Eq. (2), two parameters very similar to those found for the mononuclear parent high-spin complex [Fe(**L4**)$_3$]$^{5+}$ (Table 3).

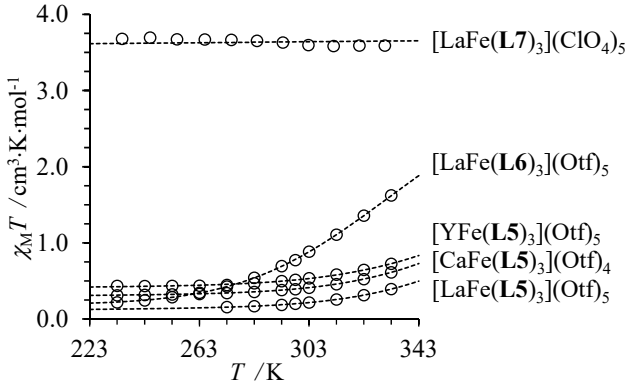

Figure 9. Corrected $\chi_M T$ products plotted as a function of the temperature for 0.01 M solution of [LaFe(**L5**)$_3$]$^{5+}$, [CaFe(**L5**)$_3$]$^{4+}$, [YFe(**L5**)$_3$]$^{5+}$, [LaFe(**L6**)$_3$]$^{5+}$ and [LaFe(**L7**)$_3$]$^{5+}$in CD_3CN. The dotted traces correspond to non-linear least-square fits obtained with Eqs (1)-(2) and using the parameters gathered in Table 3.

Accepted Manuscript

This article is protected by copyright. All rights reserved.

Table 3. Magnetic and thermodynamic parameters obtained by non-linear least-square fits using Eqs (1)-(2) for the $\chi_M T$ versus T plots recorded for the homoleptic [Fe(**L*k***)$_3$]X$_2$ complexes in solution (CD_3CN).

complexes	X	C_{hs} /cm^3·K·mol^{-1}	TIP_{hs}·10^{-6} /cm^{3}mol^{-1}	C_{ls} /cm^3·K·mol^{-1}	TIP_{ls}·10^{-6} /cm^{3}mol^{-1}	ΔH_{SCO} /kJ·mol^{-1}	ΔS_{SCO} /J·K·mol^{-1}	$T_{1/2}$ [a] /K	$x_{Fe(III)}$	Reference
[Fe(**bipy**)$_3$]X$_2$	CF_3SO_3	-	-	0.00(8)	351(55)	-	-	-	0.00	This work
[Fe(**L1a**)$_3$]X$_2$	CF_3SO_3	3.44[b]	358[b]	0.00[c]	351[c]	35.0(3)	100(1)	349(5)	0.032	This work
[Fe(**L1a**)$_3$]X$_2$	PF_6	3.44[b]	358[b]	0.00[c]	351[c]	35.7(3)	101(1)	354(5)	0.00	This work
[Fe(**L2a**)$_3$]X$_2$	CF_3SO_3	3.44[b]	358[b]	0.00[c]	351[c]	28.3(4)	91(1)	309(6)	0.01	This work
[Fe(**L2a**)$_3$]X$_2$	PF_6	3.44[b]	358[b]	0.00[c]	351[c]	28.6(3)	91.5(8)	313(4)	0.00	This work
[Fe(**L3**)$_3$]X$_2$	CF_3SO_3	3.41(5)	1321(88)	-	-	-	-	-	0.01	This work
[Fe(**L4**)$_3$]X$_2$	CF_3SO_3	3.44(2)	358(57)	-	-	-	-	-	0.00	This work
[LaFe(**L5**)$_3$]X$_5$	CF_3SO_3	3.44[b]	358[b]	0.00[c]	351[c]	37.9(5)	92(1)	412(8)	0.01[d]	This work
[YFe(**L5**)$_3$]X$_5$	CF_3SO_3	3.44[b]	358[b]	0.00[c]	351[c]	34(2)	83(5)	412(33)	0.08[d]	This work
[CaFe(**L5**)$_3$]X$_4$	CF_3SO_3	3.44[b]	358[b]	0.00[c]	351[c]	36.8(2)	90.4(6)	407(3)	0.05[d]	This work
[LaFe(**L6**)$_3$]X$_5$	CF_3SO_3	3.44[b]	358[b]	0.00[c]	351[c]	29.6(2)	86.2(5)	344(3)	0.03	This work
[LaFe(**L6**)$_3$]X$_5$	ClO_4	3.44[b]	358[b]	0.00[c]	351[c]	30.0(2)	88(1)	331(5)	-	[49d]
[LaFe(**L7**)$_3$]X$_5$	ClO_4	3.44(4)	310(15)	-	-	-	-	-	0.02	[19]

[a] $T_{1/2} = \Delta H_{SCO}/\Delta S_{SCO}$. [b] C_{hs} and TIP_{hs} found for [Fe(**L4**)$_3$](CF_3SO_3)$_2$ are used for fitting the SCO behaviors. [c] C_{ls} and TIP_{ls} found for [Fe(**bipy**)$_3$](CF_3SO_3)$_2$ are used for fitting the SCO behaviors. [d] Deduced from low-temperature data fitted for pure low-spin complex.

Accepted Manuscript

This article is protected by copyright. All rights reserved.

For $[CaFe(\mathbf{L5})_3]^{4+}$, $[YFe(\mathbf{L5})_3]^{5+}$ $[LaFe(\mathbf{L5})_3]^{5+}$ and $[LaFe(\mathbf{L6})_3]^{5+}$, the $\chi_M T$ versus T plots are diagnostic for spin-crossover processes (Figure 9), the thermodynamic characteristics of which could be extracted with Eqs (1)-(2) (see Appendix 2) and collected in Table 3. Since only a limited temperature range is available for collecting SCO data for $[CaFe(\mathbf{L5})_3]^{4+}$, $[YFe(\mathbf{L5})_3]^{5+}$and $[LaFe(\mathbf{L5})_3]^{5+}$ in solution (Figure 9), ΔH_{SCO} and ΔS_{SCO} are the only adjusted parameters within the SCO domain using Eqs (1)-(2) for these complexes, while TIP_{hs}, TIP_{ls} and $x_{Fe(III)}$ are fixed (see caption in Table 3). Taking into account that no cooperativity factor can influence mononuclear SCO processes, the known linear dependence of the van't Hoff equation correlating ΔH_{SCO} and ΔS_{SCO} with $\ln(K_{SCO})$ implies that both parameters can be obtained with a similar precision, obviously limited by experimental dispersion and by the restricted accessible temperature range.[57]

Considering that ΔH_{SCO} and ΔS_{SCO} measured for C_3-symmetrical helicates *HHH*-$[LaFe(\mathbf{L}\boldsymbol{k})_3]^{5+}$ strictly refer to pure facial isomer (**L*k*** = **L5**-**L6**), it is not so surprising that the enthalpic contributions are 1-2 kJ/mol larger than those found in related mixtures of *mer*/*fac*-$[Fe(\mathbf{L}\boldsymbol{k})_3)]^{2+}$ complexes (**L*k*** = **L1**-**L2**, Table 3) because the latter mixtures are largely dominated by the meridional isomers (see Figure S17). It is indeed the facial arrangement which benefits from the largest thermodynamic *trans*-influence (Table S13) and consequently possesses the strongest Fe-N bonds. Interestingly, the entropic contributions ΔS_{SCO} is reduced by 6-10 $J{\cdot}mol^{-1}{\cdot}K^{-1}$ in the pure facial isomer found in the $[LaFe(\mathbf{L}\boldsymbol{k})_3]^{5+}$ helicate, a trend which can be assigned to the larger dipole moments of the facial isomers (compared with the meridional isomers) and their detrimental effect on the solvation free energy changes upon molecular size expansions accompanying low-spin → high-spin transition (Eq(18), *vide supra*).[58] Let's stress here that changing the size or the charge of the innocent (*i*. *e*. non-paramagnetic) capping cations (Ca^{2+}, Y^{3+}, La^{3+}) in the helicates $[CaFe(\mathbf{L5})_3]^{4+}$, $[YFe(\mathbf{L5})_3]^{5+}$ and $[LaFe(\mathbf{L5})_3]^{5+}$ has very limited impact on the Fe^{II}-centered spin-crossover processes, a consequence of the large flexibility of the capping unit and its minor influence on the Fe^{II} coordination sphere, except for the preorganization of a single facial isomer (Figure S25).[18b],[49d],[59] Altogether, the opposite trends displayed by ΔH_{SCO} (*i*. *e*. increase) and ΔS_{SCO} (*i*. *e*. decrease) in going from the

Accepted Manuscript

This article is protected by copyright. All rights reserved.

mononuclear $[Fe(\mathbf{Lk})_3]^{2+}$ complexes (*i. e.* mixture of *mer*/*fac* isomers) to the dinuclear helicates $[LnM(\mathbf{Lk})_3]^{5+}$ (*i. e.* pure facial isomer) produces a significant shift of $T_{1/2} = \Delta H_{SCO}/\Delta S_{SCO}$ toward higher temperature ($\Delta T_{1/2}$ = 30-60 K), which eventually delays the SCO process in the pure facial isomers found in the helicates. Assuming that $[LaFe(\mathbf{L5})_3]^{5+}$ and $[LaFe(\mathbf{L6})_3]^{5+}$ are acceptable thermodynamic models for the SCO transitions occurring in *fac*-$[Fe(\mathbf{L1})_3]^{2+}$ and *fac*-$[Fe(\mathbf{L2})_3]^{2+}$ respectively, the assignment of specific spin state equilibria for the facial isomer ($K_{SCO}^{fac\text{-}Fe(\mathbf{L1})_3} = x_{hs}^{fac} / x_{hs}^{fac} = K_{SCO}^{LnFe(\mathbf{L5})_3}$ and $K_{SCO}^{fac\text{-}Fe(\mathbf{L2})_3} = x_{hs}^{fac} / x_{hs}^{fac} = K_{SCO}^{LnFe(\mathbf{L6})_3}$, Table 3) and for the meridional isomer ($K_{SCO}^{mer\text{-}Fe(\mathbf{Lk})_3} = x_{hs}^{mer} / x_{hs}^{mer}$) in the mononuclear $[Fe(\mathbf{Lk})_3]^{2+}$ complexes transforms Eq. (2) into Eq. (17) (Appendix 3).

$$\chi_M T = \left(x_{hs}^{fac} + x_{hs}^{mer}\right)\cdot\left(C_{hs} + T\cdot TIP_{hs}\right) + \left(x_{ls}^{fac} + x_{ls}^{mer}\right)\cdot\left(C_{ls} + T\cdot TIP_{ls}\right) + x_{Fe(III)}\cdot C_{Fe(III)} \quad (17)$$

The various mole fractions involved in Eq. (17) must obey the mass balance $x_{hs}^{fac} + x_{ls}^{fac} + x_{hs}^{mer} + x_{ls}^{mer} + x_{Fe(III)} = 1$, together with the thermodynamic constraint accompanying meridional $\rightarrow$ facial isomerization $K_{mer\rightarrow fac}^{Fe,\mathbf{Lk}} = \left(x_{ls}^{fac} + x_{hs}^{fac}\right) / \left(x_{ls}^{mer} + x_{hs}^{mer}\right)$ (Eq. (10) and Table S13). With this ultimate model in hand, the non-linear least-square fits of the $\chi_M T$ versus T plots recorded for the SCO processes displayed by $[Fe(\mathbf{L1a})_3]^{2+}$ and $[Fe(\mathbf{L2a})_3]^{2+}$ in acetonitrile yield the two missing parameters $\Delta H_{SCO}^{mer\text{-}Fe(\mathbf{Lk})_3}$ and $\Delta S_{SCO}^{mer\text{-}Fe(\mathbf{Lk})_3}$ (Figure 10, Table 4; see Appendix 3 for details). In all rigor, a calibration by a spectroscopic technique (ie. Mössbauer spectrometry) is necessary for the estimation of the residual fractions LS (high temperature) and HS (low temperature) which slightly modify the parameters of the fitting process (ΔH and ΔS). However, the impossibility of carrying out Mössbauer spectrometry in solution leads us to consider only the magnetic susceptibility measurements for comparison of the different compounds, what remains valid for our analysis.

Accepted Manuscript

This article is protected by copyright. All rights reserved.

Table 4. Thermodynamic parameters obtained by non-linear least-square fits using Eq. (17) for the $\chi_M T$ versus T plots recorded for the homoleptic [Fe(**L*k***)$_3$]X$_2$ complexes in solution (CD$_3$CN).

complexes	ΔH_{sco} / kJ·mol^{-1}	ΔS_{sco} / J·mol^{-1}·K^{-1}	$T_{½}$ / K	$x_{Fe(III)}$ / %	AF [c]
pyrazines					
fac-[Fe(**L1a**)$_3$]$^{2+}$ [a]	37.9(5)	92(1)	412(8)	1.16(2)	2.50·10^{-3}
mer-[Fe(**L1a**)$_3$](Otf)$_2$	35.9(6)	106(2)	339(8)	3.3(1)	1.04·10^{-2}
mer-[Fe(**L1a**)$_3$](PF$_6$)$_2$	35.9(3)	104.1(9)	345(4)	0.00(7)	5.13·10^{-3}
pyridines					
fac-[Fe(**L2a**)$_3$]$^{2+}$ [b]	29.6(2)	86.2(5)	344(3)	2.83(6)	3.89·10^{-3}
mer-[Fe(**L2a**)$_3$](Otf)$_2$	29.3(6)	97(2)	303(8)	1.4(4)	1.13·10^{-2}
mer-[Fe(**L2a**)$_3$](PF$_6$)$_2$	29.2(3)	95.0(8)	307(4)	0.0(2)	5.51·10^{-3}

[a] [LaFe(**L5**)$_3$](Otf)$_5$ is taken as model (see text). [b] [LaFe(**L6**)$_3$](Otf)$_5$ is taken as model (see text).

[c] Agreement factor $AF = (\Sigma(\chi_M T_{exp}-\chi_M T_{calc})^2/\Sigma(\chi_M T_{exp})^2)^{½}$.

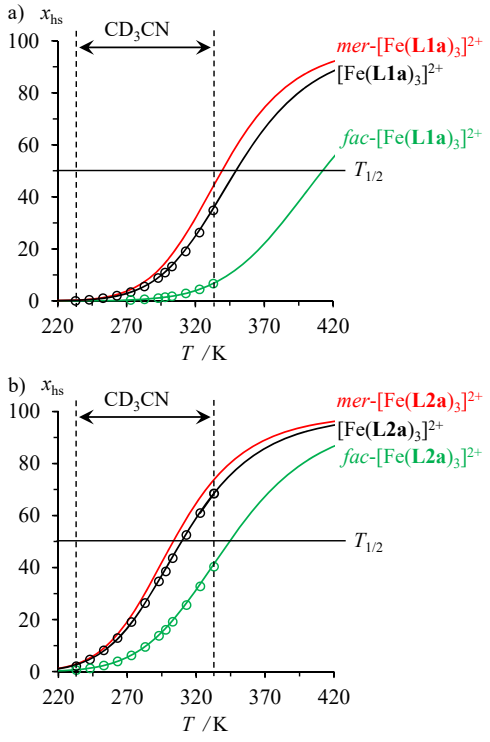

Figure 10. High-spin mole fraction (x_{hs}) as a function of the temperature for 0.01 M CD$_3$CN solution of a) [Fe(**L1a**)$_3$](CF$_3$SO$_3$)$_2$ (black) (and its partition between *fac*-[Fe(**L1a**)$_3$]$^{2+}$ (green) and *mer*-[Fe(**L1a**)$_3$]$^{2+}$ (red)) and b) [Fe(**L2a**)$_3$](CF$_3$SO$_3$)$_2$ (black) (and its partition between *fac*-[Fe(**L2a**)$_3$]$^{2+}$ (green) and *mer*-[Fe(**L2a**)$_3$]$^{2+}$ (red)) in CD$_3$CN. The traces correspond to non-linear least-square fits obtained with Eq. (17) and using the parameters gathered in Table 4.

Accepted Manuscript

This article is protected by copyright. All rights reserved.

For both pyrazine-type (**L1a**) and pyridine-type (**L2a**) ligands, the temperature $T_{1/2} = \Delta H_{SCO}/\Delta S_{SCO}$ at which $x_{hs} = x_{ls} = 0.5$ is shifted toward higher values in going from *mer*-$[Fe(\mathbf{Lk})_3]^{2+}$ to *fac*-$[Fe(\mathbf{Lk})_3]^{2+}$ (Figure 10) due to the concomitant (minor) increase of ΔH_{SCO} and decrease of ΔS_{SCO} in the facial isomer (Table 4), this whatever the helicate $[LaFe(\mathbf{L5})_3]^{5+}$, $[YFe(\mathbf{L5})_3]^{5+}$ or $[CaFe(\mathbf{L5})_3]^{4+}$ chosen for modelling *fac*-$[Fe(\mathbf{L1a})_3]^{2+}$ (Table S16). The enthalpic trend can be assigned to the minor, but non-negligible thermodynamic *trans*-influence, which strengthens the Fe-N bonds in the facial isomer, especially for *fac*-$[Fe(\mathbf{L1a})_3]^{2+}$ (Table S13). The entropic tendency is rather counter-intutive since it opposes the gain in electronic degeneracy upon spin transition, which is larger for C_3-symmetrical *fac*-$[Fe(\mathbf{Lk})_3]^{2+}$ ($\Delta S_{el}(^1A \rightarrow {}^5E) = R\ln(10) = 19.1$ J·K^{-1}·mol^{-1}) than for C_1-symmetrical *mer*-$[Fe(\mathbf{Lk})_3]^{2+}$ ($\Delta S_{el}(^1A \rightarrow {}^5A) = R\ln(5) = 13.4$ J·K^{-1}·mol^{-1}). The global decrease of the entropic contribution to the spin crossover transition occurring in *fac*-$[Fe(\mathbf{Lk})_3]^{2+}$ can be thus tentatively traced back to the change in solvation energies accompanying the 1-2 % volume expansion of the complexes (see Appendix 1). Since *mer*-$[Fe(\mathbf{Lk})_3]^{2+}$ and *fac*-$[Fe(\mathbf{Lk})_3]^{2+}$ have similar volume and charge, the dominant monopole contribution (produced by the doubly charged pseudo-spherical cations) to solvation energies would be identical for both isomers. On the contrary, the dipole contribution will be different since *fac*-$[Fe(\mathbf{Lk})_3]^{2+}$, which possess up-up-up arrangements of the three ligands (Figure 1), are expected to have large electric dipoles along the threefold axis ($\mu_{dip} = 7.5(5)$ Debye could be computed for the optimized gas-phase structure of *fac*-$[Zn(\mathbf{L1a})_3]^{2+}$).[15] On the contrary, the *mer*-$[Fe(\mathbf{Lk})_3]^{2+}$ isomers (up-up-down arrangement of the ligand strands, Figure 1) possess lower electric dipoles ($\mu_{dip} = 5.2(6)$ Debye computed for *mer*-$[Zn(\mathbf{L1a})_3]^{2+}$).[15] Rough estimations of the contribution to solvation free energy $\Delta_{solv}G$ of a dipolar guest dissolved in a dielectric continuum can be then obtained by using *Onsager* Equation (18), where $N_A = 6.022 \cdot 10^{23}$ mol^{-1} is Avogadro's number, $e = 1.602 \cdot 10^{-19}$ C is the elementary charge, $\varepsilon_0 = 8.854 \cdot 10^{-12}$ C^2·N^{-1}·m^{-2} is the vacuum permittivity, ε_r is the relative dielectric permittivity ($\varepsilon_r = 37.5$ in acetonitrile), μ_d is the dipole moment of the particle and R_i is the radius of a spherical cavity cut from the dielectric when a spherical solute is immersed into the solvent.[58]

Accepted Manuscript

This article is protected by copyright. All rights reserved.

$$\Delta_{solv}G^0 = -N_{av}\frac{\mu^2}{4\pi\varepsilon_0\left(R_i\right)^3}\cdot\left(\frac{\varepsilon_r - 1}{2\varepsilon_r + 1}\right) \quad (18)$$

Assuming that the dipole moment is similar in low-spin and high-spin configurations, the variation of free energy of solvation $\Delta\Delta_{solv}G^0 = \Delta_{solv}G^0_{hs} - \Delta_{solv}G^0_{ls}$ during the SCO transition is systematically positive since $R_{hs} > R_{ls}$ and therefore maximized for the facial isomers possessing the larger dipole moments. An exact partition of the solvation effects between enthalpic and entropic effects is currently under investigation, but beyond the scope of this contribution.

Conclusion

Chemical intuition and semi-quantitative structural criteria[7] remain the most popular and the most exploited strategies for designing novel spin-crossover complexes.[2] According that unpredictable intermolecular interactions operating in bulk solids[60] largely dominate the rational minor enthalpic and entropic tunings induced by molecular design,[61] the latter empirical approach is fully justified and leads to noticeable advances in the design of switchable and/or bistable macroscopic materials displaying positive cooperativities.[2c],[9c] However, microscopic structure-properties correlations remain attractive for pushing novel concepts into the arena of empirical exploration, this at the condition that pertinent test benches are available for evaluating which molecular effects are at the origin of specific thermodynamic trends in SCO complexes. Solution studies play a crucial role in this field since intermolecular interactions are limited to solvation energies, which display faint variations upon spin-state equilibria, thus allowing a reliable analysis of structure-properties correlations. However, molecular structure and speciation are much more challenging to address in solution compared to solid state, particularly for (semi)-labile complexes such as homoleptic $[Fe(\mathbf{L}\boldsymbol{k})_3]^{2+}$ complexes (**L*k*** = **L1**-**L4**), which are quantitatively formed only at exact stoichiometric ratio and at sufficiently high concentration in acetonitrile. Moreover, $[Fe(\mathbf{L}\boldsymbol{k})_3]^{2+}$ exist as temperature-dependent mixtures of meridional/facial isomers. If specific magnetic and thermodynamic parameters have been characterized for related homoleptic tris-didentate complexes in the solid state, where a single isomer (facial or meridional) could be crystallized by chance,[11] the use of an ultra-flexible

Accepted Manuscript

This article is protected by copyright. All rights reserved.

non-covalent lanthanide podate in *HHH*-[LnFe(**L*k***)$_3$]$^{5+}$ for modelling facial arrangement could become a novel attractive toolkit for addressing the SCO properties of these different isomers in solution. Applying this strategy, we showed here that:

1) Pyrazine is a weaker σ-donor, but a much stronger π-acceptor than pyridine for M^{II} in the [M(**L*k***)$_3$]$^{2+}$ complexes. This ultimately (and counter-intuitively) produces larger Δ_{oct}/B ratios and delayed spin crossover transitions occurring at higher temperature for **L1** or **L5**-type ligands.

2) Weak but non-negligible thermodynamic *trans*-influence enthalpically favors the formation of *fac*-[M(**L*k***)$_3$]$^{2+}$ (M = Fe^{II}, Zn^{II}), a trend offsets at room temperature by opposite entropic contributions produced by the larger dipole moment of the latter isomer. This effect is maximum for pyrazine-benzimidazole units in **L1**, which contributes to the larger ΔH_{SCO} parameters found for *fac*-[Fe(**L1**)$_3$]$^{2+}$.

3) The SCO transition temperature $T_{1/2}$ of the facial isomer is shifted by several tenths of degrees toward high values compared with the meridional isomer in solution as the result of concomitant enthalpic (*trans*-influence) and entropic (solvation) effects. Since the latter entropic effect depends on the dielectric constant of the medium (see Eq. (18)), further fine tuning could be envisioned *via* a judicious choice of the solvent.

Altogether, we are now equipped for attempting some *de novo* design of spin-crossover d-f dinuclear helicates [LnFe(**L**)$_3$]$^{5+}$, in which the facial arrangement of three homoleptic diimine units ensures transition temperatures $T_{1/2}$ below room temperature, a characteristic compatible with the optical sensing of the magnetic switch via a neighboring luminescent lanthanide in a (supra)molecular object.[10],[19]

Acknowledgements

Financial support from the Swiss National Science Foundation is gratefully acknowledged. The authors thank Dr. Sophie Michalet and Harry Théraulaz for ESI-MS analyses (Mass Spectrometry Core Facility *MZ* 2.0, University of Geneva), Jean-François Meunier and Lionel Rechignat for

Accepted Manuscript

This article is protected by copyright. All rights reserved.

SQUID measurements (Laboratory of Coordination Chemistry (LCC), Toulouse) and Kerry-Lee Buchwalder for elemental analyses.

Conflict of interest

The authors declare no conflict of interest.

Keywords: Spin transition, magnetism, thermodynamics, isomers, iron, facial-meridional

References

[1] L. Cambi, L. Szegö, *Ber. Deutsch. Chem. Ber. B* **1931**, *64*, 2591-2598.

[2] a) P. Gütlich, H. A. Goodwin, Eds, *Spin Crossover in Transition Metal Compounds I-III,* in *Top. Curr. Chem.* **2004**, *233-235*; b) A. Bousseksou, G. Molnar, G. Matouzenko, *Eur. J. Inorg. Chem.* **2004**, 4353-4369; c) M. Sorai, M. Nakano, Y. Miyazaki, *Chem. Rev.* **2006**, *106*, 976-1031; d) M. A. Halcrow, Ed., *Spin-Crossover Materials: Properties and Applications*, John Wiley & Sons Ltd, Chichester, 2013; e) D. Unruh, P. Homenya, M. Kumar, R. Sindelar, Y. Garcia, F. Renz, *Dalton Trans.* **2016**, *45*, 14008-14018; f) M. M. Khusniyarov, *Chem. Eur. J.* **2016**, *22*, 15178-15191.

[3] P. Gütlich, Y. Garcia, H. A. Goodwin, *Chem. Soc. Rev.* **2000**, *29*, 419-427.

[4] a) M. A. Halcrow, *Polyhedron* **2007**, *26*, 3523-3576; b) J. Olguin, S. Brooker, *Coord. Chem. Rev.* **2011**, *255*, 203-240; c) H. L. C. Feltham, A. S. Barltrop, S. Brooker, *Coord. Chem. Rev.* **2016**, *344*, 26-53. d) M. Attwood, S. S. Turner, *Coord. Chem. Rev.* **2017**, *353*, 247-277; d) H. S. Scott, R. W. Staniland, P. E. Kruger, *Coord. Chem. Rev.* **2018**, *362*, 24-43.

[5] a) C. K. Jorgensen, *Modern Aspects of Ligand Field Theory*, North-Holland Publishing Company, Amsterdam, London, 1971; b) T. Ishii, S. Tsuboi, G. Sakane, M. Yamashita and B. K. Breedlove, *Dalton Trans.* **2009**, 680-687.

[6] a) C. K. Jorgensen, *Oxidations Numbers and Oxidation States*, Springer Verlag, New York, 1969; b) B. N. Figgis, M. A. Hitchman, *Ligand Field Theory and Its Application*, Wiley-VCH, New Yok, Chichester, Weinheim, Brisbane, Singapore, Toronto, 2000, pp 215-221.

Accepted Manuscript

This article is protected by copyright. All rights reserved.

[7] H. Phan, J. J. Hrudka, D. Igimbayeva, L. M. L. Daku, M. Shatruk, *J. Am. Chem. Soc.* **2017**, *139*, 6437-6447.

[8] a) B. N. Figgis, M. A. Hitchman, *Ligand Field Theory and Its Application*, Wiley-VCH, New Yok, Chichester, Weinheim, Brisbane, Singapore, Toronto, 2000, pp 131-144; b) A. Trueba, P. Garcia-Fernandez, J. M. Garcia-Lastra, J. A. Aeramburu, M. T. Barriuso, M. Moreno, *J. Phys. Chem. A* **2011**, *115*, 1423-1432.

[9] a) G. Chastanet, A. B. Gaspar, J. A. Real, J.-F. Létard, *Chem. Commun.* **2001**, 819-820; b) A. B. Gaspar, V. Ksenovontov, M. Seredyuk, P. Gütlich, *Coord. Chem. Rev.* **2005**, *249*, 2661-2676; c) S. Brooker, *Chem. Soc. Rev.* **2015**, *44*, 2880-2892.

[10] a) I. Suleimanov, O. Kraieva, G. Molnar, L. Salmon, A. Bousseksou, *Chem. Commun.* **2015**, *51*, 15098-15101. b) J.-L. Wang, Q. Liu, X.-J. Lv, R.-L. Wang, C.-Y. Duan, T. Liu, *Dalton Trans.* **2016**, *45*, 18552-18558; c) B. Schäfer, T. Bauer, I. Faus, J. A. Wolny, F. Dahms, O. Fuhr, S. Lebedkin, H.-C. Wille, K. Schlage, K. Chevalier, F. Rupp, R. Diller, V. Schünemann, M. M. Kapples, M. Ruben, *Dalton Trans.* **2017**, *46*, 2289-2302; d) S. M. Fatur, S. G. Shepard, R. F. Higgins, M. P. Shores, N. H. Damrauer, *J. Am. Chem. Soc.* **2017**, *139*, 4493-4505; e) J.-L. Wang, Q. Liu, Y.-S. Meng, X. Liu, H. Zheng, Q. Shi, C.-Y. Duan, T. Liu, *Chem. Sci.* **2018**, *9*, 2892-2897; f) C. Lochenie, K. Schötz, F. Panzer, H. Kurz, M. B., F. Puchtler, S. Agarwal, P. Köhler, B. Weber, *J. Am. Chem. Soc.* **2018**, *140*, 700-709.

[11] a) J. Klingele, H. Scherer, M. Klingele, *Z. Anorg. Allg. Chem.* **2009**, *635*, 2279-2287; b) J. A. Kitchen, N. G. White, M. Boyd, B. Moubaraki, K. S. Murray, P. D. W. Boyd, S. Brooker, *Inorg. Chem.* **2009**, *48*, 6670-6679; c) D. Furushou, T. Hashibe, T. Fujinami, K. Nishi, H. Hagiwara, N. Matsumoto, Y. Sunatsuki, M. Kojima, S. Iijima, *Polyhedron* **2013**, *52*, 1489-1498; d) X.-H. Zhao, S.-L. Zhang, D. Shao, X.-Y. Wang, *Inorg. Chem.* **2015**, *54*, 7857-7867; e) W.-K. Han, Z.-H. Li, W. Zhu, T. Li, Z. Li, X. Ren, Z.-G. Gu, *Dalton Trans.* **2017**, *46*, 4218-4224.

Accepted Manuscript

This article is protected by copyright. All rights reserved.

[12] a) P. A. Anderson, T. Astley, M. A. Hitchmann, F. R. Keene, B. Moubaraki, K. S. Murray, B. W. Skelton, E. R. T. Tiekink, H. Toftlund, A. H. White, *J. Chem. Soc., Dalton Trans.* **2000**, 3505-3512; b) M. Seredyuk, M. C. Munoz, V. Ksenofontov, P. Gütlich, Y. Galyametdinov, J. A. Real, *Inorg. Chem.* **2014**, *53*, 8442-8454; c) N. Struch, N. Wagner, G. Schnakenburg, R. Weisbarth, S. Klos, J. Beck, A. Lützen, *Dalton Trans.* **2016**, *45*, 14023-14029; d) R. Kulmaczewski, O. Cespedes, M. A. Halcrow, *Inorg. Chem.* **2017**, *56*, 3144-3148.

[13] S. di Stefano, G. Ercolani, *Adv. Phys. Org. Chem.* **2016**, *50*, 1-76.

[14] a) G. Canard, S. Koeller, G. Bernardinelli, C. Piguet, *J. Am. Chem. Soc.* **2008**, *130*, 1025-1040; b) P. E. Ryan, L. Guénée, G. Canard, F. Gumy, J.-C. G. Bünzli, C. Piguet, *Inorg. Chem.* **2009**, *48*, 2549-2560; c) C. Piguet in *Handbook on the Physics and Chemistry of Rare Earths*, Vol. 47, Eds: K. A. Gschneidner Jr., J.-C. G. Bünzli and V. K. Pecharsky, Elsevier Science, Amsterdam, 2015, pp. 209-271.

[15] L. Aboshyan-Sorgho, T. Lathion, L. Guénée, C. Besnard, C. Piguet, *Inorg. Chem.* **2014**, *53*, 13093-13104.

[16] a) T. Riis-Johannessen, N. Dalla Favera, T. K. Todorova, S. M. Huber, L. Gagliardi, C. Piguet, *Chem. Eur. J.* **2009**, *15*, 12702-12718; b) C. Piguet, J.-C. G. Bünzli in *Handbook on the Physics and Chemistry of Rare Earths*, Vol. 40, Eds: K. A. Gschneidner Jr., J.-C. G. Bünzli and V. K. Pecharsky, Elsevier Science, Amsterdam, 2010, pp 301-553; c) P. E. Ryan, G. Canard, S. Koeller, B. Bocquet, C. Piguet, *Inorg. Chem.* **2012**, *51*, 10012-10024.

[17] W.-H. Sun, P. Hao, S. Zhang, Q. Shi, W. Zuo, X. Tang, *Organometallics* **2007**, *26*, 2720-2734.

[18] a) C. Piguet, J.-C. G. Bünzli, G. Bernardinelli, G. Hopfgartner, S. Petoud, O. Schaad, *J. Am. Chem. Soc.* **1996**, *118*, 6681-6697; b) C. Piguet, E. Rivara-Minten, G. Bernardinelli, J.-C. G. Bünzli, G. Hopfgartner, *J. Chem. Soc., Dalton Trans.* **1997**, 421-433.

[19] C. Edder, C. Piguet, J.-C. G. Bünzli, G. Hopfgartner, *Chem. Eur. J.* **2001**, *7*, 3014-3024.

Accepted Manuscript

This article is protected by copyright. All rights reserved.

[20] a) W. C. Wolsey, *J. Chem. Educ.* **1973**, *50*, A335-A337; b) J.-L. Pascal, F. Favier, *Coord. Chem. Rev.* **1998**, *178-180*, 865-902.

[21] a) E. R. Malinowski, D. G. Howery, *Factor Analysis in Chemistry*, Wiley, New York, Chichester, 1980; b) H. Gampp, M. Maeder, C. J. Meyer, A. Zuberbühler, *Talanta* **1986**, *33*, 943-951; c) B. R. Hall, L. E. Manck, I. S. Tidmarsh, A. Stephenson, B. F. Taylor, E. J. Blaikie, D. A. Vander Griend, M. D. Ward, *Dalton Trans.* **2011**, *40*, 12132-12145.

[22] a) H. Gampp, M. Maeder, C. J. Meyer, A. Zuberbühler, *Talanta*, **1985**, *32***,** 1133-1139; b) M. Maeder, P. King, *Analysis of Chemical Processes, Determination of the Reaction Mechanism and Fitting of Equilibrium and Rate Constants*, in Chemometrics in Practical Applications, Dr. Kurt Varmuza (Ed.), ISBN: 978-953-51-0438-4, InTech, DOI: 10.5772/31896; c) *ReactLab*^{TM} *Equilibria* (previously Specfit/32), Jplus Consulting Pty. Ltd., Palmyra WA 6957, Australia: http://jplusconsulting.com/products/reactlab-equilibria/.

[23] G. A. Bain, J. F. Berry, *J. Chem. Educ.* **2008**, *85*, 532-536.

[24] a) D. F. Evans, *J. Chem. Soc.* **1959**, 2003-2005; b) T. H. Crawford, J. Swanson, *J. Chem. Educ.* **1971**, *48*, 382-386; c) J. Löliger, R. Sheffold, *J. Chem. Educ.* **1972**, *49*, 646-647.

[25] D. S. Raiford, C. L. Fisk, E. D. Becker, *Anal. Chem.* **1979**, *51*, 2050-2051.

[26] a) M. V. Baker, L. D. Field, T. W. Hambley, *Inorg. Chem.* **1988**, *27*, 2872-2876; b) E. M. Schubert, *J. Chem. Educ.* **1992**, *69*, 62.

[27] D. H. Grant, *J. Chem. Educ.* **1995**, *72*, 39-40.

[28] C. Piguet, *J. Chem. Educ.* **1997**, *74*, 815-816.

[29] a) D. Ostfeld, I. A. Cohen, *J. Chem. Educ.* **1972**, *49*, 829; b) Y.-Z. Hu, M. H. Wilson, R. Zong, C. Bonnefous, D. R. McMillin, R. P. Thummel, *Dalton Trans.* **2005**, *2*, 354-358; c) J. England, R. Gondhia, L. Bigorra-Lopez, A. R. Petersen, A. J. P. White, G. J. P. Britovsek, *Dalton Trans.* **2009**, *27*, 5319-5334.

Accepted Manuscript

This article is protected by copyright. All rights reserved.

[30] a) SIR97 A. Altomare, M. C. Burla, M. Camalli, G. Cascarano, C. Giacovazzo, A. Guagliardi, G. Moliterni, G. Polidori, R. Spagna, *J. Appl. Cryst.* **1999**, *32*, 115-119; b) SHELXS97 G. M. Sheldrick, *Acta Crystallogr. A* **2008**, *64*, 112–122;

[31] G. M. Sheldrick, *Acta Crystallogr. Sect. C Struct. Chem.* **2015**, *71*, 3–8.

[32] SHAPE is a free software developed by M. Llunell, D. Casanova, J. Cirera, P. Alemany, S. Alvarez, and available online at http://www.ee.ub.edu/. For more information see a) M. Pinsky, D. Avnir, *Inorg. Chem.* **1998**, *37*, 5575-5582; b) S. Alvarez, D. Avnir, M. Llunell, M. Pinsky, *New J. Chem.* **2002**, *26*, 996-1009; c) D. Casanova, J. Cirera, M. Llunell, P. Alemany, D. Avnir, S. Alvarez, *J. Am. Chem. Soc.* **2004**, *126*, 1755-1763; d) J. Cirera, E. Ruiz, S. Alvarez, *Chem. Eur. J.* **2006**, *12*, 3162-3167.

[33] C. Piguet, G. Bernardinelli, G. Hopfgartner, *Chem. Rev.* **1997**, *97*, 2005-2062.

[34] a) E. A. Quadrelli, *Inorg. Chem.* **2002**, *41*, 167-169 ; b) M. Seitz, A. G. Oliver, K. N. Raymond, *J. Am. Chem. Soc.* **2007**, *129*, 11153-11160.

[35] O. Kahn, *Molecular Magnetism*, VCH Publishers, Inc., Weinhein, 1993, chap. 2.

[36] a) B. N. Figgis, *Nature* **1958**, *182*, 1568-1570; b) M. Kotani, *J. Phys. Soc. Jpn.* **1949**, *4*, 293-297.

[37] a) L. L. Martin, R. L. Martin, K. S. Murray, A. M. Sargeson, *Inorg. Chem.* **1990**, *29*, 1387-1394; b) R. Sharp, L. Lohr, J. Miller, *Prog. Nucl. Magn. Reson. Spec.* **2001**, *38*, 115-158; c) J.-P. Costes, J. M. Clemente-Juan, F. Dahan, F. Dumestre, J.-P. Tuchagues, *Inorg. Chem.* **2002**, *41*, 2886-2891; d) R. Boca, *Coord. Chem. Rev.* **2004**, *248*, 757-815.

[38] a) W. Kläui, W. Eberspach, P. Gütlich, *Inorg. Chem.* **1987**, *26*, 3977-3982; b) J. F. Berry, F. A. Cotton, T. B. Lu, C. A. Murillo, *Inorg. Chem.* **2003**, *42*, 4425-4430; c) Z. Ni, M. P. Shores, *Inorg. Chem.* **2010**, *49*, 10727-10735.

[39] L. Alderighi, P. Gans, A. Ienco, D. Peters, A. Sabatini, A. Vacca, "Hyperquad Simulation and Speciation (HySS): A Utility Program for the Investigation of Equilibria Involving Soluble and Partially Soluble Species", *Coord. Chem. Rev.* **1999**, *184*, 311-318.

Accepted Manuscript

This article is protected by copyright. All rights reserved.

[40] a) K. Nakamoto, *J. Phys. Chem.* **1960**, *64*, 1420-1425; b) S. Xu, J. E. T. Smith, J. M. Weber, *Inorg. Chem.* **2016**, *55*, 11937-11943.

[41] a) A. Ceulemans, L. G. Vanquickenborne, *J. Am. Chem. Soc.* **1981**, *103*, 2238-2241; b) T. J. Meyer, *Pure Appl. Chem.* **1986**, *58*, 1193-1206; c) J. Fan, J. Autschbach, T. Ziegler, *Inorg. Chem.* **2010**, *49*, 1355-1362.

[42] a) S. W. Benson, *J. Am. Chem. Soc.* **1958**, *80*, 5151-5154; b) G. Ercolani, C. Piguet, M. Borkovec, J. Hamacek, *J. Phys. Chem. B* **2007**, *111*, 12195-12203.

[43] a)M. Borkovec, J. Hamacek, C. Piguet, *Dalton Trans.* **2004**, 4096-4105; b) C. Piguet, *Chem. Commun.* **2010**, *46*, 6209-6231.

[44] H. Irving, R. J. P. Williams, *J. Chem. Soc.* **1953**, 3192-3210.

[45] a) A. E. Martell, R. M. Smith, R. J. Motekaitis, NIST Standard Reference Data, Gaithersburg, MD 20899, USA; b) H. Irving, D. H. Mellor, *J. Chem. Soc.* **1962**, 5217-5222.

[46] L. Helm, A. E. Merbach, *Chem. Rev.* **2005**, *105*, 1923-1959.

[47] A. B. P. Lever, *Inorganic Electronic Spectroscopy*, Elsevier, Amsterdam, London, 1984, pp 126-127.

[48] N. Triest, G. Bussiere, H. Belisle, C. Reber, *J. Chem. Educ.* **2000**, *77*, 670.

[49] a) A. T. Baker, H. A. Goodwin, A. D. Rae, *Aust. J. Chem.* **1984**, *37*, 2431-2440; b) A. T. Baker, H. A. Goodwin, *Aust. J. Chem.* **1985**, *38*, 851-863; c) C. B. J. Childs, D. C. Craig, M. L. Scudder, H. A. Goodwin, *Aust. J. Chem.* **1999**, *52*, 673-680; d) C. Edder, C. Piguet, G. Bernardinelli, J. Mareda, C. G. Bochet, J.-C. G. Bünzli, G. Hopfgartner, *Inorg. Chem.* **2000**, *39*, 5059-5073.

[50] S. M. Hart, J. C. A. Boeyens, R. D. Hancock, *Inorg. Chem.* **1983**, *22*, 982-986.

[51] a) R. J. Smithson, C. A. Kilner, A. R. Brough, M. A. Halcrow, *Polyhedron* **2003**, *22*, 725-733; b) R. J. Deeth, M. A. Halcrow, L. J. Kershaw Cook and P. R. Raithby, *Chem. Eur. J.* **2018**, *24*, 5204-5212.

Accepted Manuscript

This article is protected by copyright. All rights reserved.

[52] a) B. J. Childs, J. M. Cadogan, D. C. Craig, M. L. Scudder, H. A. Goodwin, *Aust. J. Chem.* **1997**, *50*, 129-138; b) R. Mohammed, G. Chastanet, F. Tuna, T. L. Malkin, S. A. Barrett, C. A. Kilner, J.-F. Létard, M. A. Halcrow, *Eur. J. Inorg. Chem.* **2013**, 819-831; c) R. G. Miller, S. Brooker, *Chem. Sci.* **2016**, *7*, 2501-2505.

[53] a) B. Weber, F. A. Walker, *Inorg. Chem.* **2007**, *46*, 6794-6803; b) A. A. Pavlov, G. L. Denisov, M. A. Kiskin, Y. V. Nelyubina, V. V. Novikov, *Inorg. Chem.* **2017**, *56*, 14759-14762; c) S. De, S. Tewary, D. Garnier, Y. Li, G. Gontard, L. Lisnard, A. Flambard, F. Breher, M.-L. Boillot, G. Rajaraman, R. Lescouëzec, *Eur. J. Inorg. Chem.* **2018**, 414-428.

[54] L. J. Charbonnière, A. F. Williams, C. Piguet, G. Bernardinelli, E. Rivara-Minten, *Chem. Eur. J.* **1998**, *4*, 485-493.

[55] K. H. Sugiyarto, D. C. Craig, A. D. Rae, H. A. Goodwin, *Aust. J. Chem.* **1994**, *47*, 869-890.

[56] a) S. A. Barrett, M. A. Halcrow, *RSC Adv.* **2014**, *4*, 11240-11243; b) L. J. Kershaw Cook, R. Mohammed, G. Sherbone, T. D. Roberts, S. Alvarez, M. A. Halcrow, *Coord. Chem. Rev.* **2015**, 289-290, 2-12.

[57] Once the mathematical model is fixed for a linear correlation, the two parameters can be obtained with the same accuracy, see G. Lente, I. Fabian, A. J. Poe, *New J. Chem.* **2005**, *29*, 759-760.

[58] a) L. Onsager, *J. Am. Chem. Soc.* **1936**, *58*, 1486-1492; b) D. V. Matyushov, *J. Chem. Phys.* **2004**, *120*, 1375-1382; c) L. E. Johnson, S. J. Benight, R. Barnes, B. H. Robinson, *J. Phys. Chem. B* **2015**, *119*, 5240-5250; d) L. Babel, T. N. Y. Hoang, L. Guénée, C. Besnard, T. A. Wesolowski, M. Humbert-Droz, C. Piguet, *Chem. Eur. J.* **2016**, *22*, 8113-8123.

[59] C. Piguet, E. Rivara-Minten, G. Hopfgartner, J.-C. G. Bünzli, *Helv. Chim. Acta* **1995**, *78*, 1651-1672.

[60] a) J. D. Dunitz, A. Gavezzotti, *Acc. Chem. Res.* **1999**, *32*, 677-684; b) J. D. Dunitz, *Chem. Commun.* **2003**, 545-548; c) G. R. Desiraju, *Angew. Chem. Int. Ed.* **2007**, *46*, 8342-8356.

Accepted Manuscript

This article is protected by copyright. All rights reserved.

[61] a) L. Salmon, B. Donnadieu, A. Bousseksou, J.-P. Tuchagues, *C. R. Acad. Sci. Paris* **1999**, *IIc*, 305-309; b) M. Mikolasek, G. Félix, W. Nicolazzi, G. Molnar, L. Salmon, A. Bousseksou, *New J. Chem.* **2014**, *38*, 1834-1839; c) M. Mikolasek, W. Nicolazzi, F. Terki, G. Molnar, A. Bousseksou, *Phys. Chem. Chem. Phys.* **2017**, *19*, 12276-12281.

TOC

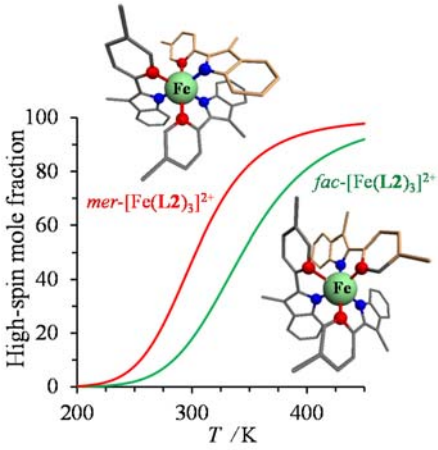

Though many pseudo-octahedral non-symmetrical homoleptic tris-diimine Fe^{II} spin crossover complexes $[Fe\mathbf{L}_3]^{z+}$ have been designed for exploring magnetic bistability and switching, specific characteristics assigned to meridional/facial isomers are essentially missing. This work proposes a strategy for overcoming this limitation.

Accepted Manuscript

This article is protected by copyright. All rights reserved.